# Linking the Signaling Cascades and Dynamic Regulatory Networks Controlling Stress Responses

Anthony Gitter, Miri Carmi, Naama Barkai, and Ziv Bar-Joseph

## Supplementary Information

## Supplementary Results

### Short model details and support

Because TFs that are active along a regulatory path are typically active at many splits along that path, Fig. 2A only displays TFs the first time they are active along a path. Supplementary Fig. S1 shows the full set of TF annotations for the short model. Supplementary Tables S1 and S2 contain the full set of targets and internal nodes in the short model as well as the external sources that support them. Our literature search was not exhaustive, and in particular we did not investigate proteins for which there was already other evidence of HOG pathway involvement. When SDREM is run on the short expression data and protein-DNA edges are not included in the interaction network, a smaller network is predicted (Supplementary Fig. S3). Without protein-DNA edges in the signaling pathways, the predicted TFs and internal nodes still significantly overlap with the gold standard (p-values $1.03 \times 10^{-3}$ and $1.97 \times 10^{-6}$, respectively). These PPI-only SDREM predictions were similar to the original predictions with 85% of the PPI-only predictions appearing in the original model.

**Supplementary Table S1. Short model targets.** The KEGG, *Science Signaling*, and other HOG models columns indicate whether the predicted TF is in the gold standard. The other HOG models column summarizes the literature-based pathway models (Hohmann et al. 2007; Hohmann 2009; Krantz et al. 2009; de Nadal and Posas 2010; Rodríguez-Peña et al. 2010). The sorbitol screen (Hillenmeyer et al. 2008) column contains the lowest p-value for the gene across all replicates. The SGD column indicates whether the TF was annotated with decreased resistance to hyperosmotic stress in the *Saccharomyces* Genome Database. Double horizontal lines separate predictions that are in the HOG gold standard, have some other form of HOG or osmotic stress response support, or have no known osmotic stress association.

| **Gene** | **ORF name** | **KEGG** | ***Science Signaling*** | **Other HOG models** | **Sorbitol screen** | **SGD** | **Literature** |
|---|---|---|---|---|---|---|---|
| Hot1 | YMR172W | N | Y | Y | $1.72 \times 10^{-6}$ | N | |
| Msn2 | YMR037C | Y | Y | Y | $8.85 \times 10^{-3}$ | N | |
| Msn4 | YKL062W | Y | Y | Y | $7.02 \times 10^{-4}$ | N | |
| Sko1 | YNL167C | N | Y | Y | N/A | N | |
| Aft2 | YPL202C | N | N | N | $5.51 \times 10^{-3}$ | N | Aft2 has been implicated as a TF that activates salt stress genes (Miller et al. 2011) |
| Cin5 | YOR028C | N | N | N | $5.65 \times 10^{-7}$ | N | Cin5 deletion mutants have been found to exhibit growth sensitivity to osmotic shock, and Cin5 induction peaks 30 to 60 minutes after exposure to moderate NaCl-induced stress (Nevitt et al. 2004). Bound by Hog1 under osmotic stress (Pokholok et al. 2006). |
| Ime1 | YJR094C | N | N | N | $4.15 \times 10^{-5}$ | N | |
| Pdr1 | YGL013C | N | N | N | $3.66 \times 10^{-5}$ | N | |
| Rox1 | YPR065W | N | N | N | $2.10 \times 10^{-4}$ | N | Rox1 is one of 20 genes that is both directly bound by Sko1 and induced at least threefold in response to osmotic stress (Proft et |

| | | | | | | | |
|---|---|---|---|---|---|---|---|
| | | | | | | | al. 2005). |
| Sok2 | YMR016C | N | N | N | $7.94 \times 10^{-11}$ | Y | |
| Spt23 | YKL020C | N | N | N | $3.78 \times 10^{-10}$ | N | |
| Yap6 | YDR259C | N | N | N | $2.13 \times 10^{-3}$ | N | Yap6 is a TF associated with osmotic stress response (Ni et al. 2009). |
| Dig1 | YPL049C | N | N | N | $3.11 \times 10^{-2}$ | N | |
| Gts1 | YGL181W | N | N | N | $2.00 \times 10^{-3}$ | N | |
| Phd1 | YKL043W | N | N | N | $1.94 \times 10^{-2}$ | N | |
| Rap1 | YNL216W | N | N | N | N/A | N | Rap1 may play a role in regulating ribosomal protein genes in response to osmotic stress, but not as significantly as Ifh1 (Wade et al. 2004). |
| Stb1 | YNL309W | N | N | N | N/A | N | |
| Ste12 | YHR084W | N | N | N | N/A | N | When Hog1 or Pbs2 is deleted Ste12 is activated by osmotic stress (O'Rourke et al. 2002). |
| Swi5 | YDR146C | N | N | N | $3.89 \times 10^{-1}$ | N | |

**Supplementary Table S2. Short model internal nodes.** See Supplementary Table S1 for column descriptions.

| Gene | ORF name | KEGG | *Science Signaling* | Other HOG models | Sorbitol screen | SGD | Literature |
|---|---|---|---|---|---|---|---|
| Cdc24 | YAL041W | N | N | Y | N/A | N | |
| Hog1 | YLR113W | Y | Y | Y | $1.00 \times 10^{-20}$ | Y | |
| Pbs2 | YJL128C | Y | Y | Y | $1.00 \times 10^{-20}$ | Y | |
| Ste11 | YLR362W | Y | Y | Y | N/A | Y | |
| Ste20 | YHL007C | Y | Y | Y | $6.33 \times 10^{-1}$ | Y | |
| Ypd1 | YDL235C | Y | Y | Y | N/A | N | |
| Aft1 | YGL071W | N | N | N | $7.51 \times 10^{-1}$ | Y | Aft1 has been implicated as a TF that activates salt stress genes (Miller et al. 2011) |
| Asf1 | YJL115W | N | N | N | $7.96 \times 10^{-1}$ | N | Asf1 reassembles chromatin following hyperosmotic-stress-induced transcription (Klopf et al. 2009). |
| Bem1 | YBR200W | N | N | N | 1.00 | N | Bem1 contributes to Ste20's function in the HOG pathway (Winters and Pryciak 2005). |
| Cdc28 | YBR160W | N | N | N | N/A | N | Osmotic stress decreases the kinase activity of the Cln3-Cdc28 complex (Bellí et al. 2001). |
| Cks1 | YBR135W | N | N | N | N/A | N | Cks1 is salt sensitive (Yu and Reed 2004). |
| Cln2 | YPL256C | N | N | N | $2.15 \times 10^{-1}$ | N | Cln2 is downregulated in osmotic stress conditions (Bellí et al. 2001). |
| Dig2 | YDR480W | N | N | N | $2.03 \times 10^{-5}$ | N | |
| Far1 | YJL157C | N | N | N | $5.83 \times 10^{-4}$ | Y | |
| Gal11 | YOL051W | N | N | N | $1.25 \times 10^{-1}$ | N | Deletion of Mediator complex members including Gal11 revealed that Mediator is essential for gene expression in response to osmotic stress (Zapater et al. 2007). |
| Hht1 | YBR010W | N | N | N | $8.05 \times 10^{-6}$ | N | |
| Kss1 | YGR040W | N | N | N | $3.86 \times 10^{-3}$ | N | Although Kss1 is a MAPK in the filamentous growth pathway, it can |

| | | | | | | | |
|---|---|---|---|---|---|---|---|
| | | | | | | | also be activated by osmotic stress (Hao et al. 2008). |
| Las17 | YOR181W | N | N | N | N/A | Y | |
| Med2 | YDL005C | N | N | N | N/A | N | Deletion of Mediator complex members including Med2 revealed that Mediator is essential for gene expression in response to osmotic stress (Zapater et al. 2007). |
| Nrg1 | YDR043C | N | N | N | $4.78 \times 10^{-2}$ | N | Nrg1 mutants show increased osmotic stress resistance (Vyas et al. 2005). |
| Pcl2 | YDL127W | N | N | N | $1.06 \times 10^{-2}$ | N | A quintuple deletion of Pcl1,2-type cyclins including Pcl2 exhibit a growth defect in a high salt medium (Lee et al. 1998). |
| Rsp5 | YER125W | N | N | N | N/A | N | Rsp5 deletion reduces transcription of stress response genes in osmotic stress conditions (Haitani et al. 2006). |
| Rvs167 | YDR388W | N | N | N | $8.35 \times 10^{-1}$ | Y | Rvs167 mutants exhibit stronger actin cytoskeleton abnormalities in the presence of salt (Bauer et al. 1993). |
| Sir3 | YLR442C | N | N | N | N/A | N | Osmotic stress affects Sir3 telomere binding (Mazor and Kupiec 2009). |
| Skn7 | YHR206W | N | N | N | $2.54 \times 10^{-2}$ | N | Skn7 is a TF associated with osmotic stress response (Ni et al. 2009). |
| Ste7 | YDL159W | N | N | N | N/A | N | Ste7 is phosphorylated following HOG pathway activation (Shock et al. 2009). |
| Tec1 | YBR083W | N | N | N | $2.74 \times 10^{-1}$ | N | HOG pathway activation inhibits Tec1 DNA binding (Shock et al. 2009). |
| Fkh2 | YNL068C | N | N | N | $3.91 \times 10^{-1}$ | N | Fkh2 has not been experimentally validated, but was previously |

| | | | | | | | |
|---|---|---|---|---|---|---|---|
| | | | | | | | predicted to be a significant hyperosmotic shock TF (Lin et al. 2007). |
| Fus3 | YBL016W | N | N | N | N/A | N | When Hog1 or Pbs2 is deleted Fus3 is activated by osmotic stress (O'Rourke et al. 2002). |
| Hap4 | YKL109W | N | N | N | $8.78 \times 10^{-2}$ | N | |
| Hhf1 | YBR009C | N | N | N | $8.86 \times 10^{-3}$ | N | |
| Hhf2 | YNL030W | N | N | N | N/A | N | |
| Hht2 | YNL031C | N | N | N | $3.44 \times 10^{-1}$ | N | |
| Kti12 | YKL110C | N | N | N | $5.79 \times 10^{-1}$ | N | |
| Rpo21 | YDL140C | N | N | N | N/A | N | |
| Srb5 | YGR104C | N | N | N | $4.53 \times 10^{-1}$ | N | |
| Ste5 | YDR103W | N | N | N | N/A | N | Ste5 facilitates osmotic stress-related MAPK pathway cross-talk in Pbs2 mutants (Flatauer et al. 2005). |
| Swi4 | YER111C | N | N | N | $1.75 \times 10^{-1}$ | N | Temperature sensitivity of Swi4 mutants is suppressed by sorbitol (Madden et al. 1997). |
| Swi6 | YLR182W | N | N | N | $7.38 \times 10^{-1}$ | N | |

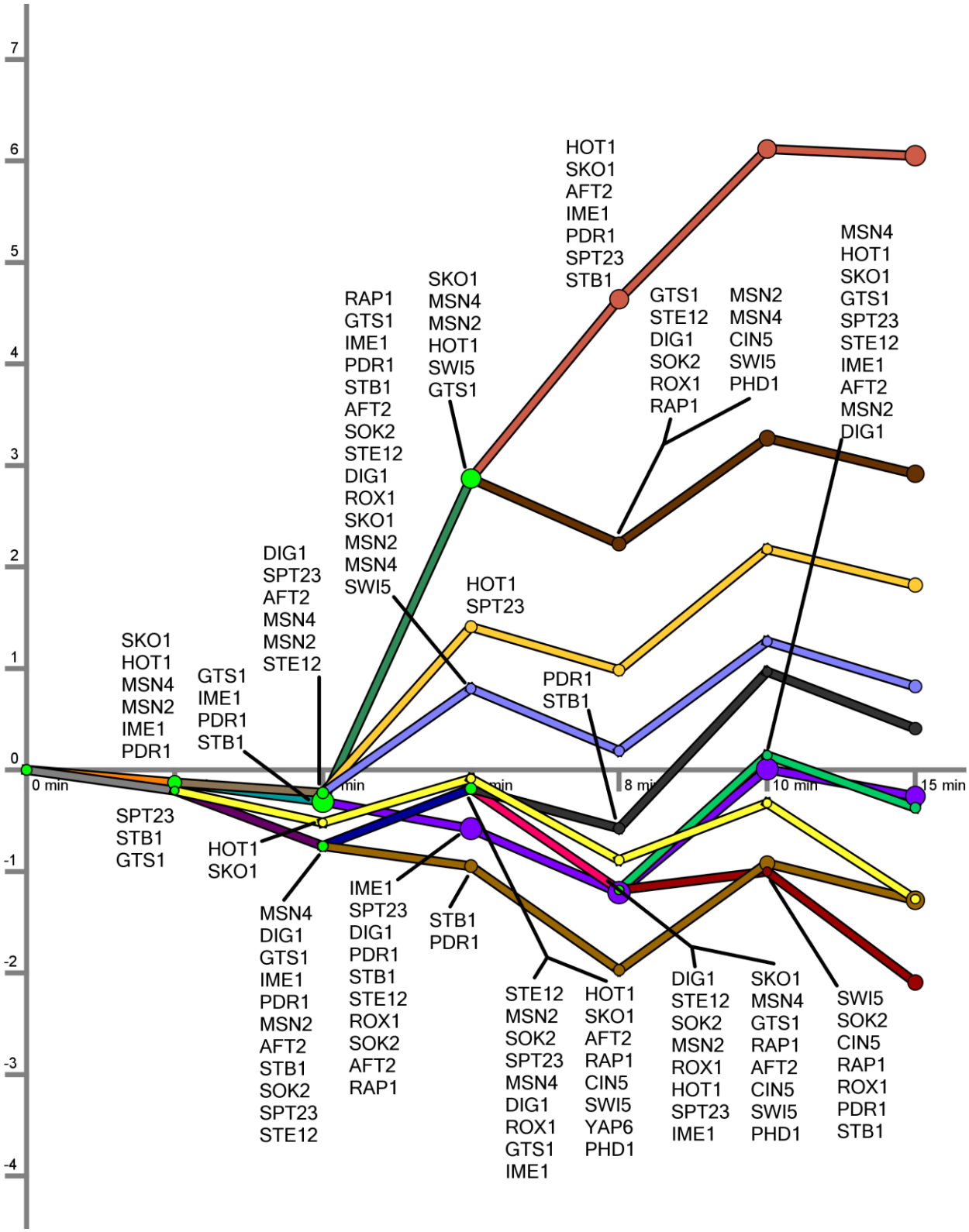


**Supplementary Figure S1. Short model active TFs**

**HOG gold standard**

Supplementary Table S3 presents the entire HOG gold standard, composed of figures from KEGG (Kanehisa and Goto 2000), the *Science Signaling* Database of Cell Signaling (http://stke.sciencemag.org/cgi/cm/stkecm;CMP_14620), and several literature sources (Hohmann et al. 2007; Hohmann 2009; Krantz et al. 2009; de Nadal and Posas 2010; Rodríguez-Peña et al. 2010). Supplementary Fig. S2 emphasizes the diversity among these seven gold standard models. Only 9 of the 42 proteins are present in all of the gold standard sources. Fifteen proteins appear in only one source, indicating that there may be less certainty that these proteins are truly HOG pathway members.

**Supplementary Table S3. Complete HOG gold standard.** All 42 members of the HOG gold standard are listed, including the sources, and are sorted in descending order by the number of databases or literature sources they appear in. TFs are denoted with 'Y' in the TF column.

| Gene | ORF name | TF | KEGG | *Sci. Sig.* | Hohmann *et al* 2007 | Hohmann 2009 | Krantz *et al* 2009 | de Nadal & Posas 2010 | Rodríguez-Peña *et al* 2010 |
|---|---|---|---|---|---|---|---|---|---|
| Hog1 | YLR113W | N | X | X | X | X | X | X | X |
| Pbs2 | YJL128C | N | X | X | X | X | X | X | X |
| Sho1 | YER118C | N | X | X | X | X | X | X | X |
| Sln1 | YIL147C | N | X | X | X | X | X | X | X |
| Ssk1 | YLR006C | N | X | X | X | X | X | X | X |
| Ssk2 | YNR031C | N | X | X | X | X | X | X | X |
| Ste11 | YLR362W | N | X | X | X | X | X | X | X |
| Ste20 | YHL007C | N | X | X | X | X | X | X | X |
| Ypd1 | YDL235C | N | X | X | X | X | X | X | X |
| Cdc42 | YLR229C | N | | X | X | X | X | X | X |
| Ssk22 | YCR073C | N | | X | X | X | X | X | X |
| Msb2 | YGR014W | N | | X | | X | X | X | X |
| Ste50 | YCL032W | N | | X | X | | X | X | X |
| Hot1 | YMR172W | Y | | X | | X | X | | X |
| Msn2 | YMR037C | Y | X | X | | | X | | X |
| Msn4 | YKL062W | Y | X | X | | | X | | X |
| Opy2 | YPR075C | N | | | X | | X | X | X |
| Ptc1 | YDL006W | N | | X | X | X | X | | |
| Ptp2 | YOR208W | N | | X | X | X | X | | |
| Ptp3 | YER075C | N | | X | X | X | X | | |
| Hkr1 | YDR420W | N | | | | X | | X | X |
| Sko1 | YNL167C | Y | | X | | | X | | X |
| Cdc24 | YAL041W | N | | | X | | X | | |
| Cla4 | YNL298W | N | | | X | X | | | |
| Msn1 | YOL116W | Y | | X | | | X | | |
| Rck2 | YLR248W | N | | X | | | X | | |
| Smp1 | YBR182C | Y | | | | | X | | X |
| Act1 | YFL039C | N | | X | | | | | |
| Ctt1 | YGR088W | N | X | | | | | | |
| Eft1 | YOR133W | N | | X | | | | | |
| Eft2 | YDR385W | N | | X | | | | | |
| Glo1 | YML004C | N | X | | | | | | |
| Gpd1 | YDL022W | N | | X | | | | | |
| Mcm1 | YMR043W | Y | X | | | | | | |
| Nbp2 | YDR162C | N | | | | | X | | |
| Ptc2 | YER089C | N | | | | | X | | |
| Ptc3 | YBL056W | N | | | | | X | | |
| Rck1 | YGL158W | N | | | | | X | | |
| Rpd3 | YNL330C | N | | X | | | | | |

| | | | | | | | | | |
|---|---|---|---|---|---|---|---|---|---|
| Sin3 | YOL004W | N | | X | | | | | |
| Ssn6 | YBR112C | N | | X | | | | | |
| Tup1 | YCR084C | N | | X | | | | | |

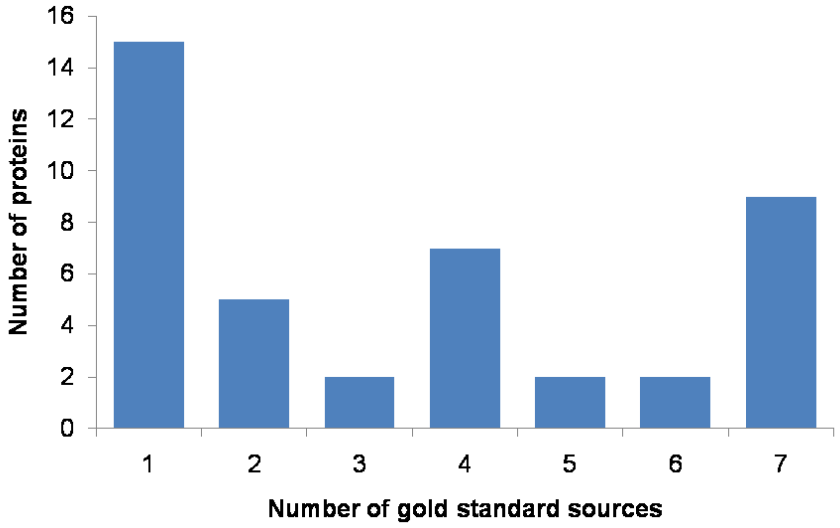


**Supplementary Figure S2. HOG gold standard source agreement.** The histogram shows how many HOG proteins appear in the specified number of gold standard sources (i.e. databases or HOG literature).

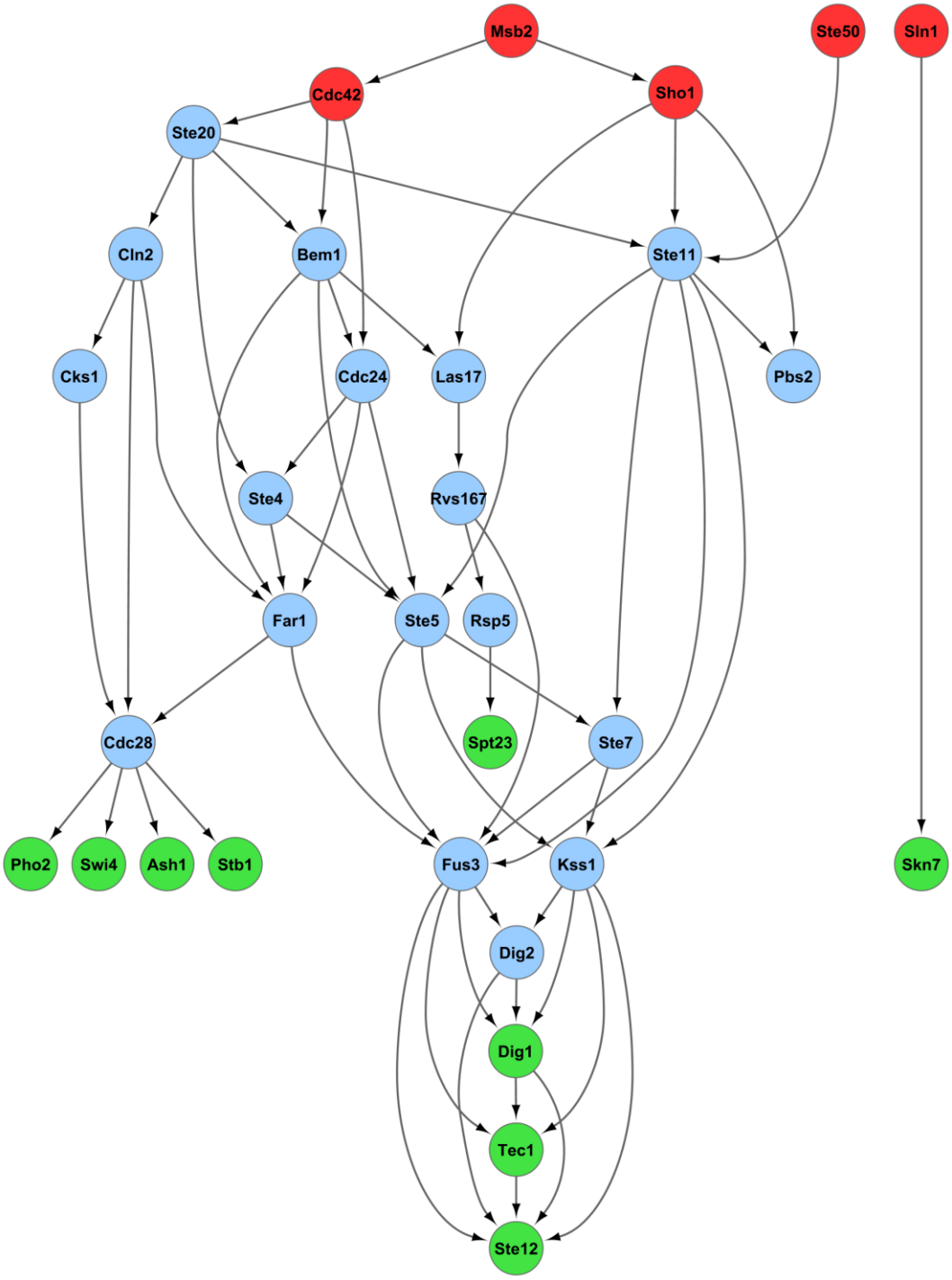


**Supplementary Figure S3. Short model signaling network without protein-DNA edges.**

Only proteins that interact with other high-confidence predictions are shown (7 are excluded).

**Long model details and support**

Fig. 3A only displays TFs the first time they are active along a path except for Hog1 and Sko1, which are shown a second time along the uppermost regulatory path to emphasize the connection between the signaling and regulatory components. Supplementary Fig. S4 provides the full set of TF annotations for the long model. Fig. 3B does not include the targets Gal4 and Sfp1 because they are connected to the sensory proteins via intermediate nodes whose scores fell below our threshold for inclusion in the model. Nevertheless, these targets are still well-connected to the source nodes. Supplementary Tables S4 and S5 contain the full set of targets and internal nodes in the long model as well as the external sources that support them.

To test whether some of the secondary TFs are likely to be controlled transcriptionally instead of by signaling cascades, we examined the subset of target TFs that are only active at the late time points (15 minutes or later). Of the 8 TFs meeting this criterion, 5 (Gcn4, Pdr1, Phd1, Sok2, and Swi5) are indeed differentially expressed in the long gene expression dataset at or before the time point where they are predicted to regulate their bound genes. These 5 TFs are also connected to the sources via paths that include one or more protein-DNA binding edges suggesting that they participate in the stress response due to transcriptional activation. Specifically, for all 8 of the late TFs, more than 50% of all paths from sources to them include at least one protein-DNA interaction. In contrast, the early TFs (those that are first active before 15 minutes) tend to be connected via paths with far fewer protein-DNA edges. Five of the 20 early TFs are primarily connected to sources with paths that contain only PPI, and one of them (Skn7) is only connected to the sources via PPIs.

To further investigate the putative transcriptional activation of the late TFs, we reran SDREM on the long expression data but left the protein-DNA binding edges out of the interaction network (these interactions were still used when learning the regulatory paths). Gcn4, Pdr1, and Phd1 are no longer predicted in this setting, which suggests that the transcriptional component of the interaction network is required for their activation. This alternate PPI-only long model is still significantly representative of the HOG pathway (p-values of 0.0100 and $8.24 \times 10^{-8}$ for the TF and signaling protein overlaps with the gold standard, respectively). The PPI-only model constructed contained 51 proteins overall, the same number as the original long model, and they had 34 proteins in common (67%).

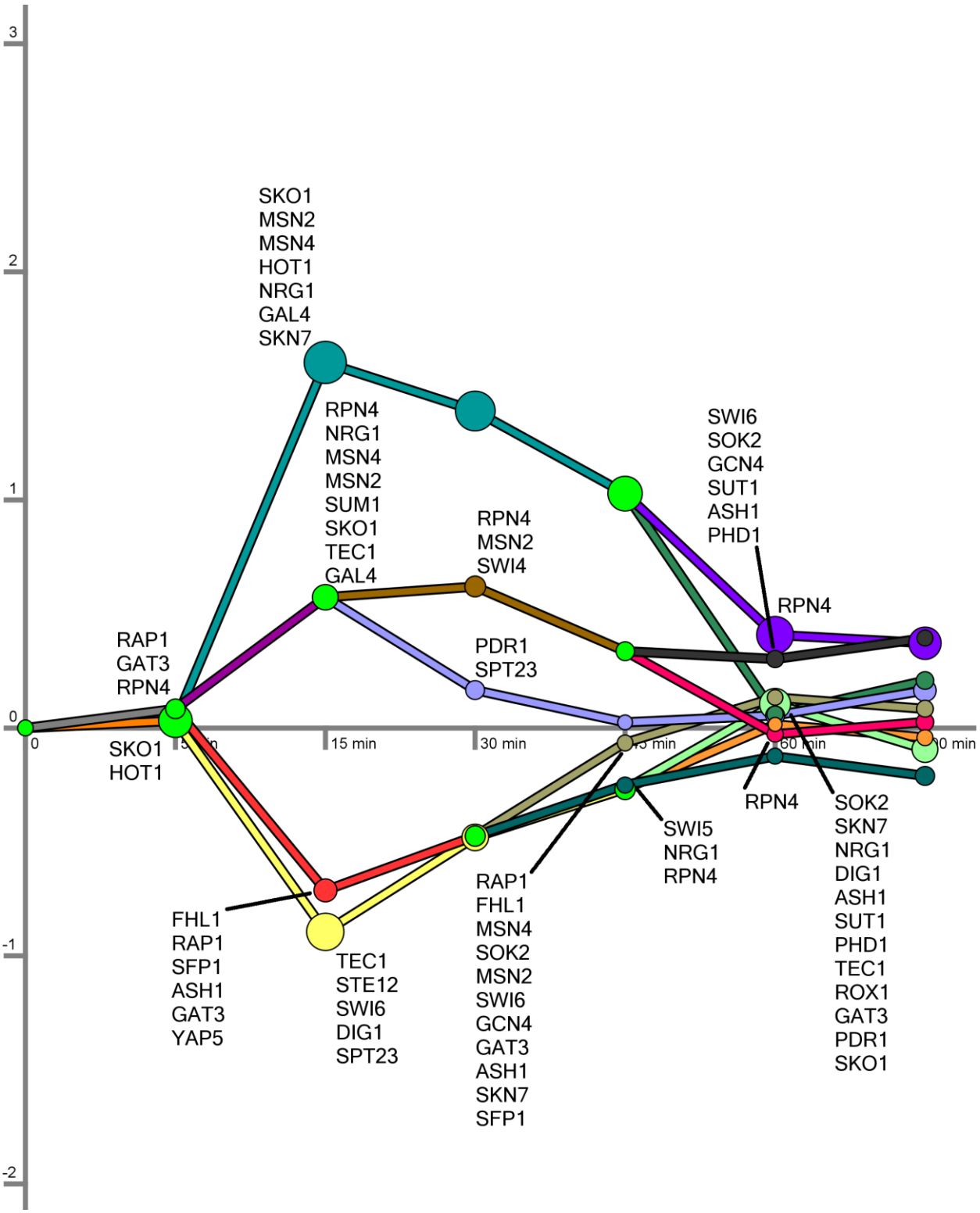


**Supplementary Figure S4. Long model active TFs**

**Supplementary Table S4. Long model targets.** See Supplementary Table S1 for column descriptions.

| Gene | ORF name | KEGG | *Science Signaling* | Other HOG models | Sorbitol screen | SGD | Literature |
|---|---|---|---|---|---|---|---|
| Hot1 | YMR172W | N | Y | Y | $1.72 \times 10^{-6}$ | N | |
| Msn2 | YMR037C | Y | Y | Y | $8.85 \times 10^{-3}$ | N | |
| Msn4 | YKL062W | Y | Y | Y | $7.02 \times 10^{-4}$ | N | |
| Sko1 | YNL167C | N | Y | Y | N/A | N | |
| Gcn4 | YEL009C | N | N | N | $1.90 \times 10^{-5}$ | N | NaCl exposure leads to translational activation of Gcn4 (Goossens et al. 2001). |
| Nrg1 | YDR043C | N | N | N | $4.78 \times 10^{-2}$ | N | Nrg1 mutants show increased osmotic stress resistance (Vyas et al. 2005). |
| Pdr1 | YGL013C | N | N | N | $3.66 \times 10^{-5}$ | N | |
| Rox1 | YPR065W | N | N | N | $2.10 \times 10^{-4}$ | N | Rox1 is one of 20 genes that is both directly bound by Sko1 and induced at least threefold in response to osmotic stress (Proft et al. 2005). |
| Skn7 | YHR206W | N | N | N | $2.54 \times 10^{-2}$ | N | Skn7 is a TF associated with osmotic stress response (Ni et al. 2009). |
| Sok2 | YMR016C | N | N | N | $7.94 \times 10^{-11}$ | Y | |
| Spt23 | YKL020C | N | N | N | $3.78 \times 10^{-10}$ | N | |
| Sut1 | YGL162W | N | N | N | $5.57 \times 10^{-2}$ | Y | |
| Tec1 | YBR083W | N | N | N | $2.74 \times 10^{-1}$ | N | HOG pathway activation inhibits Tec1 DNA binding (Shock et al. 2009). |
| Ash1 | YKL185W | N | N | N | $2.36 \times 10^{-1}$ | N | |
| Dig1 | YPL049C | N | N | N | $3.11 \times 10^{-2}$ | N | |
| Fhl1 | YPR104C | N | N | N | N/A | N | Fhl1 may play a role in regulating ribosomal protein genes in response to osmotic stress, but not as significantly as Ifh1 (Wade et al. 2004). |
| Gal4 | YPL248C | N | N | N | $2.39 \times 10^{-4}$ | N | |
| Gat3 | YLR013W | N | N | N | $5.76 \times 10^{-4}$ | N | |
| Phd1 | YKL043W | N | N | N | $1.94 \times 10^{-2}$ | N | |

| | | | | | | | |
|---|---|---|---|---|---|---|---|
| Rap1 | YNL216W | N | N | N | N/A | N | Rap1 may play a role in regulating ribosomal protein genes in response to osmotic stress, but not as significantly as Ifh1 (Wade et al. 2004). |
| Rpn4 | YDL020C | N | N | N | $6.00 \times 10^{-2}$ | N | Rpn4 has not been experimentally validated, but was previously predicted to be a significant hyperosmotic shock TF (Wu et al. 2008). |
| Sfp1 | YLR403W | N | N | N | 1.00 | N | Motif correlation suggests Sfp1 may have a role in osmotic stress response (Ni et al. 2009). |
| Ste12 | YHR084W | N | N | N | N/A | N | When Hog1 or Pbs2 is deleted Ste12 is activated by osmotic stress (O'Rourke et al. 2002). |
| Sum1 | YDR310C | N | N | N | $2.75 \times 10^{-1}$ | N | |
| Swi4 | YER111C | N | N | N | $1.75 \times 10^{-1}$ | N | Temperature sensitivity of Swi4 mutants is suppressed by sorbitol (Madden et al. 1997). |
| Swi5 | YDR146C | N | N | N | $3.89 \times 10^{-1}$ | N | |
| Swi6 | YLR182W | N | N | N | $7.38 \times 10^{-1}$ | N | |
| Yap5 | YIR018W | N | N | N | $4.92 \times 10^{-3}$ | N | |

**Supplementary Table S5. Long model internal nodes.** See Supplementary Table S1 for column descriptions.

| Gene | ORF name | KEGG | *Science Signaling* | Other HOG models | Sorbitol screen | SGD | Literature |
|---|---|---|---|---|---|---|---|
| Cdc24 | YAL041W | N | N | Y | N/A | N | |
| Hog1 | YLR113W | Y | Y | Y | $1.00 \times 10^{-20}$ | Y | |
| Ste11 | YLR362W | Y | Y | Y | N/A | Y | |
| Ste20 | YHL007C | Y | Y | Y | $6.33 \times 10^{-1}$ | Y | |
| Ypd1 | YDL235C | Y | Y | Y | N/A | N | |
| Aft1 | YGL071W | N | N | N | $7.51 \times 10^{-1}$ | Y | Aft1 has been implicated as a TF that activates salt stress genes (Miller et al. 2011) |
| Aft2 | YPL202C | N | N | N | $5.51 \times 10^{-3}$ | N | Aft2 has been implicated as a TF that activates salt stress genes (Miller et al. 2011) |
| Asf1 | YJL115W | N | N | N | $7.96 \times 10^{-1}$ | N | Asf1 reassembles chromatin following hyperosmotic-stress-induced transcription (Klopf et al. 2009). |
| Bem1 | YBR200W | N | N | N | 1.00 | N | Bem1 contributes to Ste20's function in the HOG pathway (Winters and Pryciak 2005). |
| Cdc28 | YBR160W | N | N | N | N/A | N | Osmotic stress decreases the kinase activity of the Cln3-Cdc28 complex (Bellí et al. 2001). |
| Cln2 | YPL256C | N | N | N | $2.15 \times 10^{-1}$ | N | Cln2 is downregulated in osmotic stress conditions (Bellí et al. 2001). |
| Dig2 | YDR480W | N | N | N | $2.03 \times 10^{-5}$ | N | |
| Far1 | YJL157C | N | N | N | $5.83 \times 10^{-4}$ | Y | |
| Kss1 | YGR040W | N | N | N | $3.86 \times 10^{-3}$ | N | Although Kss1 is a MAPK in the filamentous growth pathway, it can also be activated by osmotic stress (Hao et al. 2008). |
| Sir3 | YLR442C | N | N | N | N/A | N | Osmotic stress affects Sir3 telomere binding (Mazor and Kupiec 2009). |
| Ste7 | YDL159W | N | N | N | N/A | N | Ste7 is phosphorylated following HOG pathway |

| | | | | | | | |
|---|---|---|---|---|---|---|---|
| | | | | | | | activation (Shock et al. 2009). |
| Yap6 | YDR259C | N | N | N | $2.13 \times 10^{-3}$ | N | Yap6 is a TF associated with osmotic stress response (Ni et al. 2009). |
| Fus3 | YBL016W | N | N | N | N/A | N | When Hog1 or Pbs2 is deleted Fus3 is activated by osmotic stress (O'Rourke et al. 2002). |
| Gts1 | YGL181W | N | N | N | $2.00 \times 10^{-3}$ | N | |
| Rad53 | YPL153C | N | N | N | N/A | N | |
| Ste4 | YOR212W | N | N | N | N/A | N | |
| Ste5 | YDR103W | N | N | N | N/A | N | Ste5 facilitates osmotic stress-related MAPK pathway cross-talk in Pbs2 mutants (Flatauer et al. 2005). |
| Yap7 | YOL028C | N | N | N | $2.14 \times 10^{-4}$ | N | |

**Comparison to HOG pathway literature**

Although many of the edges between correctly predicted HOG gold standard members are oriented properly as well (Fig. 2B and 3B), there are cases where the inferred orientation is inconsistent with the HOG literature. Both the short and long models contain the predicted edge Ste11→Ste20. However, the gold standard reveals that Ste20→Ste11 is the true orientation (de Nadal and Posas 2010).

Fifteen proteins in the HOG gold standard, including one TF, are only annotated as HOG pathway members in a single source (Supplementary Table S3). Due to this lack of consensus, it is reasonable to believe that these proteins are less likely than the others to be involved in the HOG pathway or at the very least play peripheral roles. Interestingly, all 15 proteins are excluded from the short and long model predictions, and the gold standard overlaps are accordingly more significant when considering only gold standard proteins that are cited in multiple sources.

SDREM is designed to discover directed cascades between the upstream sources and the inferred active TFs. Therefore, it is unable to recover pathway members that are further upstream of the given sources, which explains the absence of Opy2 and Hkr1 in SDREM's predictions. Ptc2, Ptc3, Ptp2, and Ptp3 are HOG members that are not between the sources and TFs in the gold standard diagrams. Unlike Ptc2 and Ptc3, Ptp2 and Ptp3 are actually on a small number of source-target paths in the short and long models' oriented networks, but their node scores are 0, signifying that they are only found on low-confidence paths. Similarly, gold standard members Eft1 and Eft2 are not included in either osmotic stress model because they are not on any source-target paths in these models. This is consistent with the *Science Signaling* HOG pathway diagram, the only gold standard source that contains these two proteins, in which they are downstream of Hog1 but not upstream of any HOG pathway TFs.

Because the HOG gold standard only incorporates literature that provides a network diagram of the HOG pathway, we also compared our predictions with other recent HOG pathway evidence that is not reflected in the gold standard. Mas *et al* (Mas et al. 2009) explored Hog1's targeting of the RSC complex, a phenomenon missed in the SDREM models. Zapater *et al* (Zapater et al. 2007) studied Hog1's role in the recruitment of SAGA, Mediator, and Pol II in osmotic stress conditions, and identified Mediator complex genes that exhibit osmotic stress sensitivity. Of these, SDREM predicted *GAL11* and *MED2* but did not recover *PGD1* or *SRB4*. Kim and Shah (Kim and Shah 2007) identified new Hog1 substrates Krs1, Tdh3, Hsp26, and Shm2 that SDREM did not predict.

**Microscopy and FACS**

Some of the cell boundaries in the microscopy image were ambiguous, and the corresponding cells were excluded from our localization analysis. Supplementary Fig. S5 shows the regions of interest (ROIs) that were drawn on the cells that had clearly defined boundaries. Our supporting website contains the original images, images after ImageJ (Abramoff et al. 2004) processing, ROI files that can be loaded into ImageJ, and the standard deviations of the pixel intensities of all cells included in the analysis.

Although Cin5 exhibited statistically significant differential nuclear localization in the images shown in Fig. 4A and Supplementary Fig. S5, this was not the case for all images analyzed. A Cin5 image from 6 minutes after treatment had a p-value of 0.491. However, additional later images from the 40 and 50 minute time points yielded p-values of $5.54 \times 10^{-6}$ and 0.0579, respectively, and were more consistent with the results reported in the main text. This indicates that at the earlier time point, at which time SDREM predicts Cin5 is active (Fig. 2A), Cin5 had not yet localized to the nucleus in response to the osmotic stress. We believe the difference in timing could be due to differences in experimental procedures and conditions between our microscopy analysis and the gene expression dataset. Whereas we applied 1M sorbitol as the osmotic stress, the expression dataset utilized in the short model used 0.4M NaCl (Romero-Santacreu et al. 2009).

The fluorescence-activated cell sorting experiments validated not only the osmotic stress relevance of the SDREM predictions Rox1 and Gcn4, but also the timing of their involvement. The elevated Rox1 protein levels were detected 30 minutes after treatment, supporting SDREM's

predictions that it is active from 8 minutes onward in the short model and as late as 45 minutes in the long model. Gcn4's differential protein expression was detected 1 hour after treatment, consistent with the prediction that Gcn4 is active at the latest divergence point in the long model.

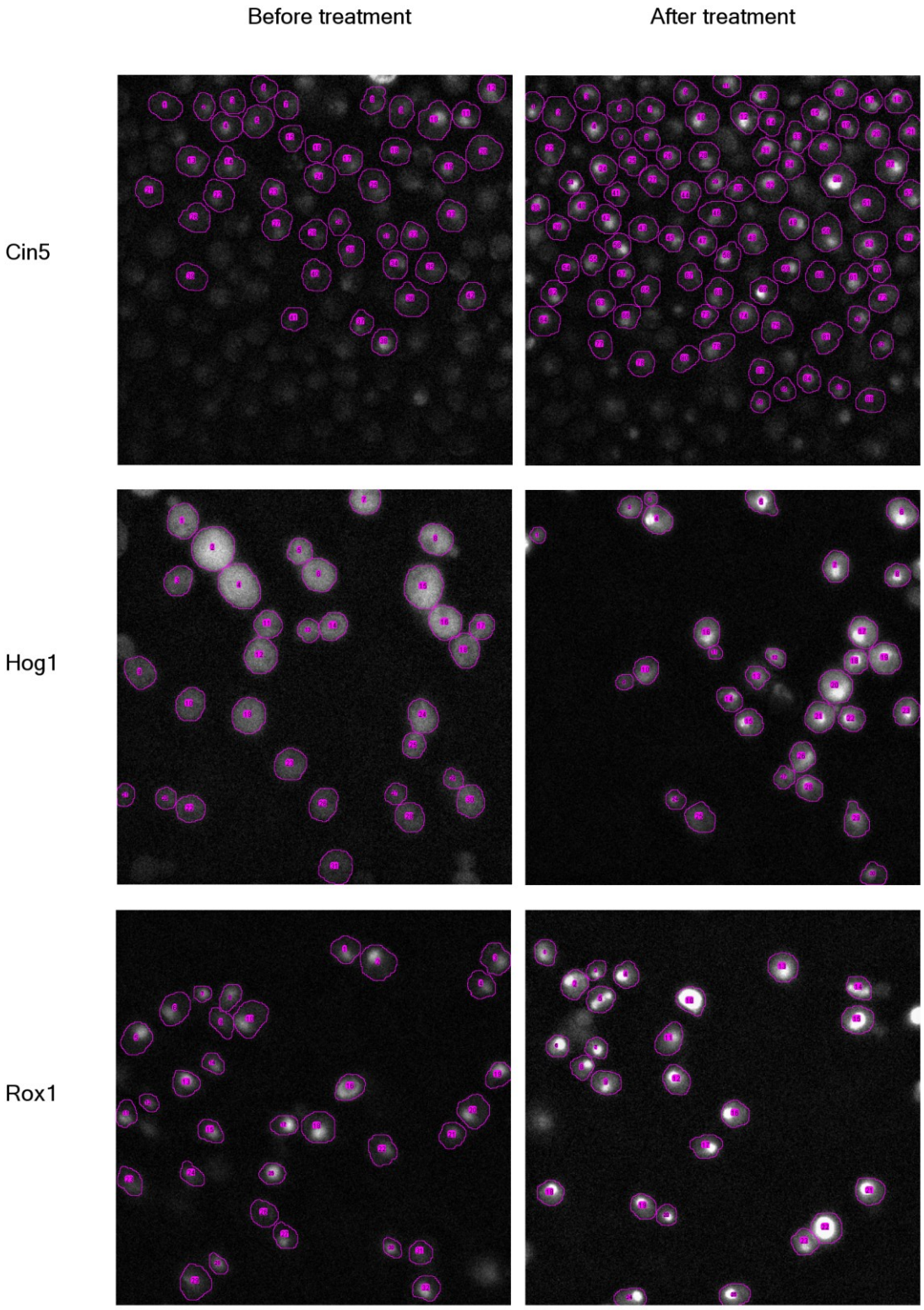


**Supplementary Figure S5. Differential nuclear localization after treatment with sorbitol.**

ROIs for cells with discernable boundaries are drawn in purple and numbered.

**Extended discussion of knockout results**

The genes we deleted were selected from the short model (Fig. 5A), but half of these nodes were present in the long network model as well (Supplementary Fig. S7A). The others were still present in some directed source-target paths, but fell below our threshold for inclusion among the highest-confidence predictions. Supplementary Fig. S7B shows the long model's regulatory paths whose genes significantly overlap with the knockout-affected genes after filtering environmental stress response (ESR) genes (Gasch et al. 2000). Supplementary Table S21 (Excel spreadsheet) provides the details of these overlaps for the short and long models including p-values. For both the short and long models, the significant knockout overlaps when the general stress response genes are not filtered are a superset of the filtered knockouts (Supplementary Fig. S6 and S8 and Supplementary Table S21). In all cases, the number of regulatory paths that are enriched with one or more knockouts is significant (Supplementary Table S6).

To more directly connect our knockout results to the predicted signaling pathways, we examined the TFs controlling the regulatory paths whose genes were significantly affected by the KO experiments. In addition to Asf1 (main text), we found several other cases where the loss of a signaling protein affects paths controlled by the downstream TFs in our oriented network. One such example involves Bem1. The genes that are differentially repressed after *BEM1* deletion in sorbitol significantly overlap path 7 in the long model (Supplementary Fig. S7B), a path on which genes are repressed at 5 minutes and then gradually recover after 15 minutes. SDREM predicts five TFs that are actively controlling genes on this path – Ste12, Tec1, Swi6, Dig1, and

Spt23 – and all five are indeed downstream of Bem1 in the oriented network (Supplementary Fig. S7A).

The genes affected by the *GAL11* KO further validate our predictions. Differentially expressed genes in the *gal11Δ* mutant significantly overlap with five paths in the short model (Fig. 5B). Of these, all but path 8 are controlled in part by Pdr1 early in the response (Supplementary Fig. S1), the only TF downstream of Gal11 in the high-confidence short model network (Fig. 5A). In fact, Pdr1 is directly bound by Gal11 in the oriented network. Rvs167 is upstream of 15 TFs in the short model, which explains why its deletion affects so many regulatory paths (Fig. 5B). The majority of the TFs controlling these paths are downstream of Rvs167 in the oriented network. For instance, 6 of the 7 TFs controlling path 1's split from path 2 are downstream of Rvs167. Additional examples exist as well, and as a whole our knockouts support our predictions in both the short and long models.

Although we were able to use the oriented network to explain many of the effects we observed when predicted signaling proteins were deleted, in some cases the abundance of paths involving the deleted node impaired these efforts. Especially for proteins like Bem1 that are further upstream in the signaling network and directly interact with the sensory proteins (Fig. 5A and Supplementary Fig. S7A), there are many TFs that are downstream of them in the network (Supplementary Table S21). Thus, there is ambiguity when determining exactly how the deletion impacted gene expression because any of these TFs could have been affected by the deletion, but for any given TF there are typically other parallel paths that do not involve the deleted node. Similarly, many regulatory paths are partially controlled by a large number of TFs,

and in almost all cases at least some of these TFs are downstream of each of our deletions (Supplementary Table S21). The degree of overlap between the downstream TFs and TFs on a regulatory path alone is not predictive of whether the deletion will significantly affect the regulatory path. Furthermore, any errors in the network orientation can impair our ability to explain the observed knockout effects.

In general, the differentially activated genes after a knockout overlapped the upper regulatory paths and repressed genes overlapped lower paths. We can explain this phenomenon in many cases, but it is nevertheless counterintuitive. One would expect to see more cases where the positive regulators downstream of the deleted protein are deactivated after the knockout, which causes the genes on that path to be differentially repressed instead of activated.

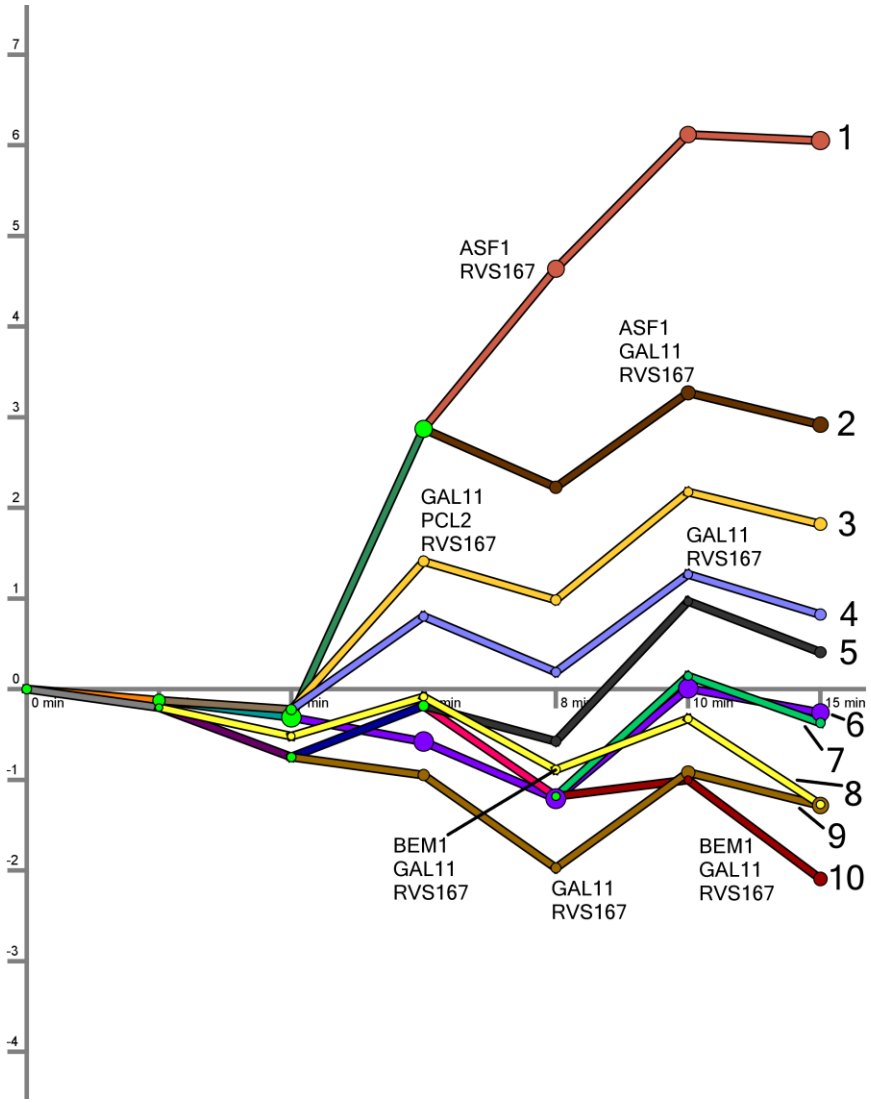


**Supplementary Figure S6. Knockouts affecting short model regulatory paths without ESR filtering**

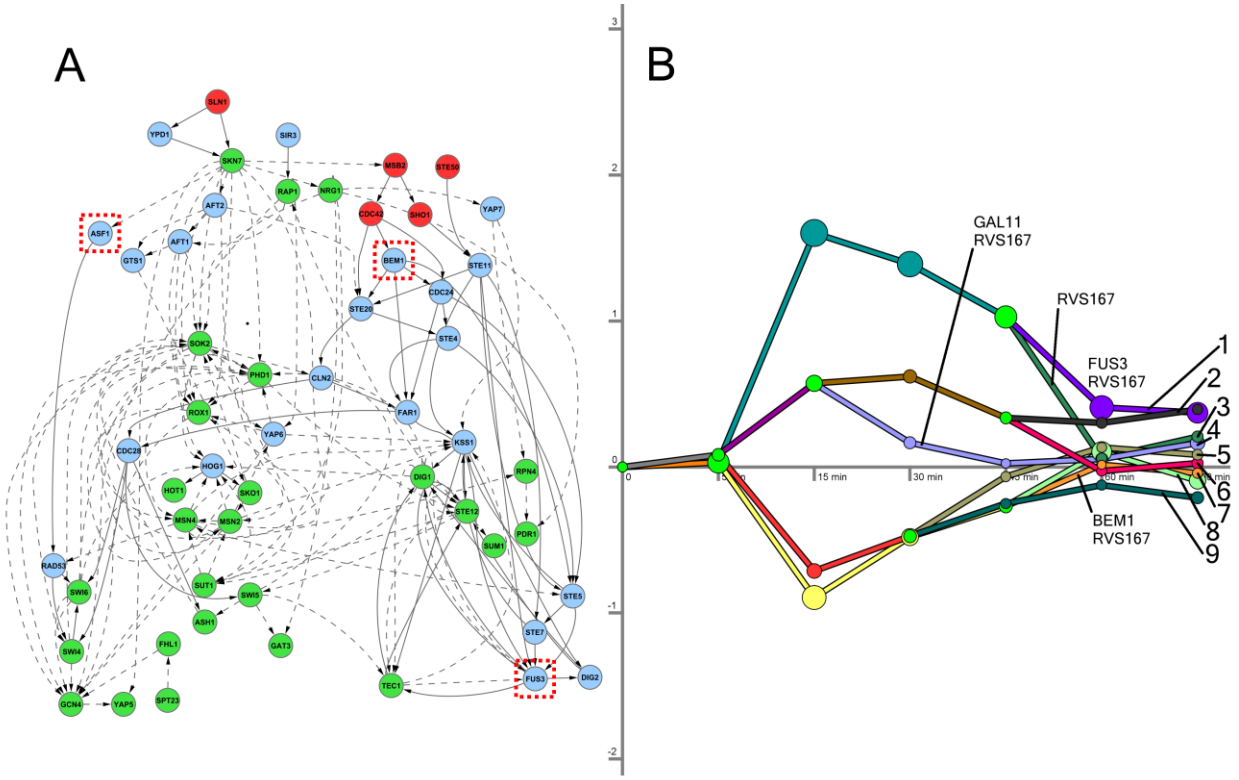


**Supplementary Figure S7. Knockouts affect downstream expression of genes on the recovered regulatory paths in the long model.** A) The positions of the deleted genes that are also in the long model. B) Four knockouts significantly affected the genes assigned to the regulatory paths in the long model. Numbered paths are annotated with the knockouts where we found significant overlap between path members and knockout-affected genes after filtering ESR genes.

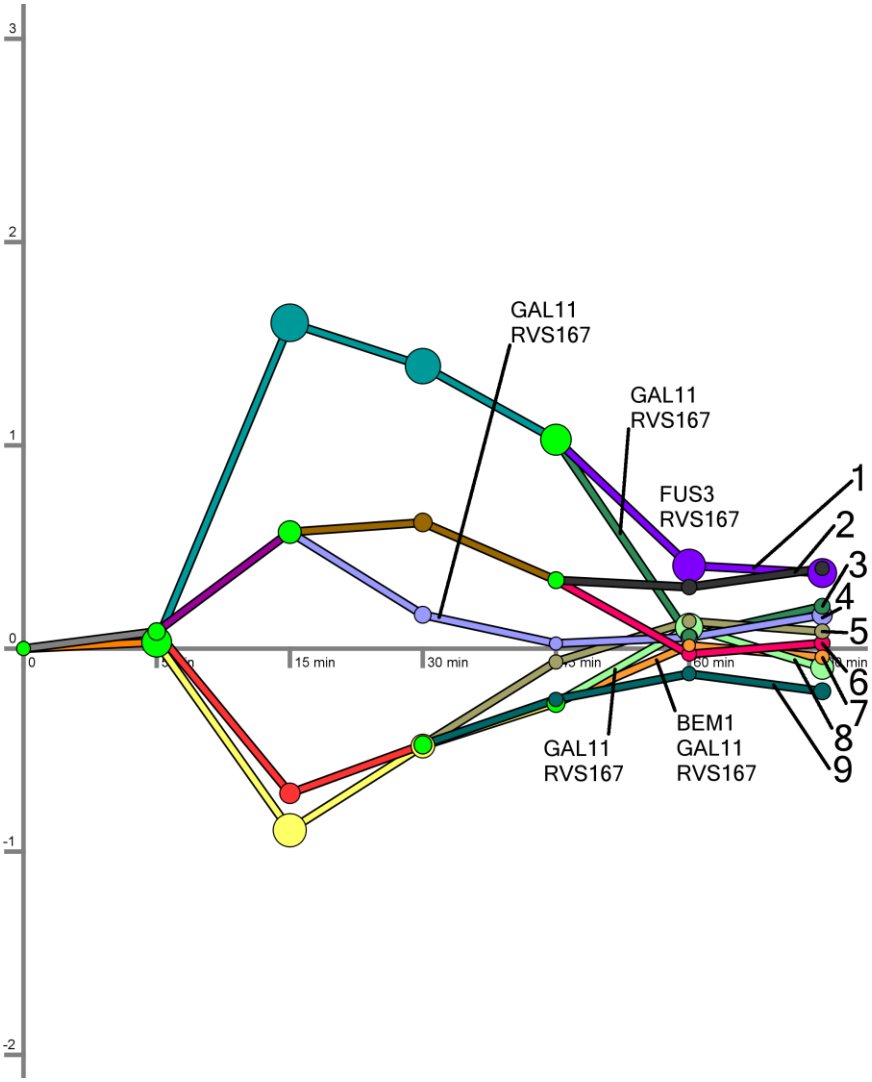


**Supplementary Figure S8. Knockouts affecting long model regulatory paths without ESR filtering**

**Supplementary Table S6. Random regulatory path enrichment.** For the short and long model, genes were randomly assigned to regulatory paths and the enrichment of the knockout-affected genes was calculated (Supplementary Methods). The number of true regulatory paths that are enriched is shown along with the number of times out of 100,000 trials that the specified number of random paths are enriched. Regardless of whether ESR genes are filtered, the resulting empirical p-values are significant.

| **Model** | Short | Short | Long | Long |
|---|---|---|---|---|
| **ESR filtered** | Yes | No | Yes | No |
| **Actual paths enriched** | 7 | 7 | 4 | 5 |
| **0 random paths enriched count** | 76353 | 72268 | 74408 | 73906 |
| **1 random paths enriched count** | 21147 | 24217 | 22732 | 23060 |
| **2 random paths enriched count** | 2359 | 3246 | 2692 | 2863 |
| **3 random paths enriched count** | 137 | 263 | 164 | 169 |
| **4 random paths enriched count** | 4 | 6 | 4 | 2 |
| **5 random paths enriched count** | 0 | 0 | 0 | 0 |
| **6 random paths enriched count** | 0 | 0 | 0 | 0 |
| **7 random paths enriched count** | 0 | 0 | 0 | 0 |
| **8 random paths enriched count** | 0 | 0 | 0 | 0 |
| **9 random paths enriched count** | 0 | 0 | 0 | 0 |
| **10 random paths enriched count** | 0 | 0 | N/A | N/A |
| **p-value** | $< 10^{-5}$ | $< 10^{-5}$ | $4 \times 10^{-5}$ | $< 10^{-5}$ |

**Confirmation of TF activity timing**

We previously discussed how the genes affected by *BEM1*'s deletion significantly overlap genes on path 7 in the long model and how the TFs downstream of Bem1 in the network control this path. Because hundreds of genes are repressed at the split at 5 minutes on this path, at least some of these TFs must be exerting a negative regulatory influence. However, our knockout results suggest that a subset of these TFs, possibly including the repressors, also control the restoration of gene expression to its steady state levels. The evidence of this is twofold. First, DREM predicts that some of the TFs controlling the downward path at the 5 minute split also control the *upward* path at 60 minutes when this path diverges into paths 7 and 8 (Supplementary Fig. S4).

This subset includes at least one TF traditionally considered to be a transcriptional repressor, Dig1 (Kusari et al. 2004). Moreover, when Bem1 is deleted, genes that are differentially *repressed* significantly overlap path 7, which means they either return to prestress levels more slowly than in wild type cells or not at all. Gene expression levels in the *bem1Δ* mutant strain were measured 30 minutes after sorbitol treatment, which supports the possibility that *BEM1*'s knockout severs the connection to the downstream TFs that are responsible for gene expression recovery after the initial repression at 5 minutes. Therefore, the *BEM1* knockout demonstrates that the time at which TFs are activated along this regulatory path was predicted correctly.

**Literature support for validated proteins**

We have shown that 3 of the 4 predicted TFs we investigated experimentally – Cin5, Gcn4, and Rox1 – localized to the nucleus and/or increased in expression in response to osmotic stress. Previous work provides further support for some of these findings and indicates that this activation may be important for overcoming sorbitol-induced stress. For example, *cin5Δ* mutants have been found to exhibit growth sensitivity to osmotic shock, and *CIN5* induction peaks 30 to 60 minutes after exposure to moderate NaCl-induced stress (Nevitt et al. 2004). Gcn4 has also been shown to play a role in salt-induced stress. Following NaCl exposure, mutations that incite Gcn4 activity also increase sensitivity to salt (Goossens et al. 2001). Osmotic stress mRNA synthesis analysis also reported Gcn4 as a regulator of salt stress genes (Miller et al. 2011).

A few of the signaling proteins we validated using knockouts were similarly identified as playing diverse roles in the osmotic stress response. Single and double knockouts revealed that Asf1 operates together with Rtt109 and in parallel with Arp8 to reassemble chromatin following

hyperosmotic stress-induced transcription (Klopf et al. 2009). Bem1's involvement in the HOG pathway is tightly coupled with Cdc42, which was selected as a source protein in our study, and Ste20, a kinase recovered in both the short and long models. Binding domain mutations revealed that both Bem1 and Cdc42 independently contribute to Ste20's function in the HOG pathway. Whereas single Bem1 or Cdc42 binding domain mutations yielded only partial defects in osmoresistance, a double mutation generated a much stronger phenotype (Winters and Pryciak 2005). In both of our network models, we recover the correct orientations of the Bem1→Ste20 and Cdc42→Ste20 PPI.

Genes affected by the *RVS167* knockout in sorbitol had the strongest overlaps with the regulatory paths. Under normal growth conditions, *rvs167Δ* mutants display slight deregulation of the actin cytoskeleton. However, in the presence of NaCl, the actin cytoskeleton of the mutant strain is completely deregulated and exhibits many abnormalities (Bauer et al. 1993). Although our single knockout only weakly confirmed Pcl2's involvement in the HOG pathway, a study by Lee *et al* (Lee et al. 1998) provides insight into this result. They found that a mutant strain in which *PCL2* was deleted was able to colonize in a high salt environment, but a quintuple deletion of Pcl1,2-type cyclins (*pcl1Δ pcl2Δ clg1Δ pcl5Δ pcl9Δ*) failed to grow on this medium. Redundancy among these cyclins obscured the salt sensitivity phenotype in the single deletion. The fact that our algorithm correctly recovered Pcl2 as an osmotic stress participant despite the weak support in its single knockout affirms our strategy to rely on dynamic gene expression data instead of knockouts for model inference. Interestingly, it was also reported that the Pcl2-Pho85 kinase phosphorylates Rvs167 (Lee et al. 1998). Much like *RVS167* deletion strains, the

quintuple Pcl1,2-type cyclin deletion exhibited abnormalities in the actin cytoskeleton that were more pronounced in the presence of salt.

**MAPK pathway cross-talk**

Extensive efforts have been made to understand the mechanisms that prevent cross-talk in yeast MAPK signaling pathways. Although the filamentous growth and pheromone-response share many members with the HOG pathway (Kanehisa and Goto 2000), activation of the respective MAPKs and downstream genes is quite specific. McClean *et al* reported that cross-talk between the HOG and pheromone pathways is filtered via mutual inhibition between Hog1 and Fus3, the MAPK in the pheromone pathway, and suggested that such mutual inhibition may be utilized in maintaining specificity of other MAPK pathways as well (McClean et al. 2007). Despite the MAPK pathway specificity in wild type cells (McClean et al. 2007), when Hog1 and the HOG pathway MAPK kinase (MAPKK) Pbs2 are mutated, Fus3 is activated by osmotic stress (O'Rourke et al. 2002). This is also the case for Ste12, a member of the filamentous growth and pheromone pathways (O'Rourke et al. 2002) that was predicted as an osmotic stress responder by SDREM. Similarly, in *pbs2Δ* strains, Ste5, a pheromone pathway member also included in our predictions, facilitates MAPK pathway cross-talk (Flatauer et al. 2005). Interestingly, other predictions that are primarily members of the filamentous growth and/or pheromone pathways have been reported to be affected by osmotic stress in wild type cells. These include the filamentous growth MAPK Kss1, the MAPKK Ste7, and the TF Tec1 (Hao et al. 2008; Shock et al. 2009).

Although there is evidence that the six aforementioned proteins have osmotic stress affiliations in either wild type or mutant strains, their inclusion in SDREM's models suggests that it can have difficulty distinguishing between MAPK pathways. Because our network orientation objective function promotes multiple parallel paths between sources and targets and some proteins (e.g. Cdc42, Msb2, Sho1, Ste11, Ste20, and Ste50) are common to multiple MAPK pathways, the algorithm predicts paths through these other MAPK pathway members. For example, in the final oriented network in the short model all of the most relevant HOG TFs (Hot1, Msn2, Msn4, and Sko1) can be connected to the source proteins via short, high-confidence paths through Fus3. Thus, the sophisticated cross-talk prevention mechanisms are unable to be recovered from the PPI and transcriptional data alone.

**Target of rapamycin (TOR) model**

The second stress response we studied with SDREM is the target of rapamycin (TOR) signaling pathway. Although yeast contains two complexes, TORC1 and TORC2, in which the Tor proteins are members, only TORC1 is inhibited by the drug rapamycin (Zaman et al. 2008). Thus, we used the five TORC1 complex members as the sources in our TOR pathway modeling: Kog1, Lst8, Tco89, Tor1, and Tor2 (Zaman et al. 2008) (Supplementary Fig. S9). Tor2 is only a TORC1 complex member in the absence of Tor1, but we include both proteins as sources. TORC1 has been shown to respond to not only rapamycin but also caffeine (Kuranda et al. 2006), nitrogen source quality (Zaman et al. 2008), and other stimuli.

The TOR response expression data (Urban et al. 2007) contained measurements at 20, 30, 60, 90, 120, and 180 minutes. Unlike the long osmotic stress expression dataset, the genes differentially

expressed in the TOR response generally remained activated or repressed for the full 3 hours and did not return to steady state during this period (Supplementary Fig. S10). Along with the extensive TF-gene binding data from cells grown in rich media (MacIsaac et al. 2006), SDREM was also provided rapamycin-specific data for 14 TFs previously implicated in the TOR response (Harbison et al. 2004).

Despite the prior evidence for these TFs' TOR involvement, conventional TOR pathway representations contain very limited knowledge of the downstream TFs. One model (Zaman et al. 2008) contains only Gln3, Msn2, Msn4, and Sfp1, and SGD shows no TFs annotated with the Gene Ontology (Ashburner et al. 2000) term 'TOR signaling cascade' (http://www.yeastgenome.org/cgi-bin/GO/goTerm.pl?goid=31929). In contrast, SDREM predicts that 23 TFs are active regulators in the TOR pathway (Supplementary Fig. S10), and of these only Sfp1 is a member of the previous TOR models. Nevertheless, we found support for 17 of these predictions (74%) in the two aforementioned TOR pathway models, rapamycin screens (Chan et al. 2000; Xie et al. 2005; Hillenmeyer et al. 2008), a set of genes curated by SGD that have a rapamycin resistance phenotype (http://www.yeastgenome.org/cgi-bin/phenotype/phenotype.fpl?property_value=rapamycin), and/or previous literature (Supplementary Table S8). We refer to this collection of evidence (excluding the literature) as our extended gold standard.

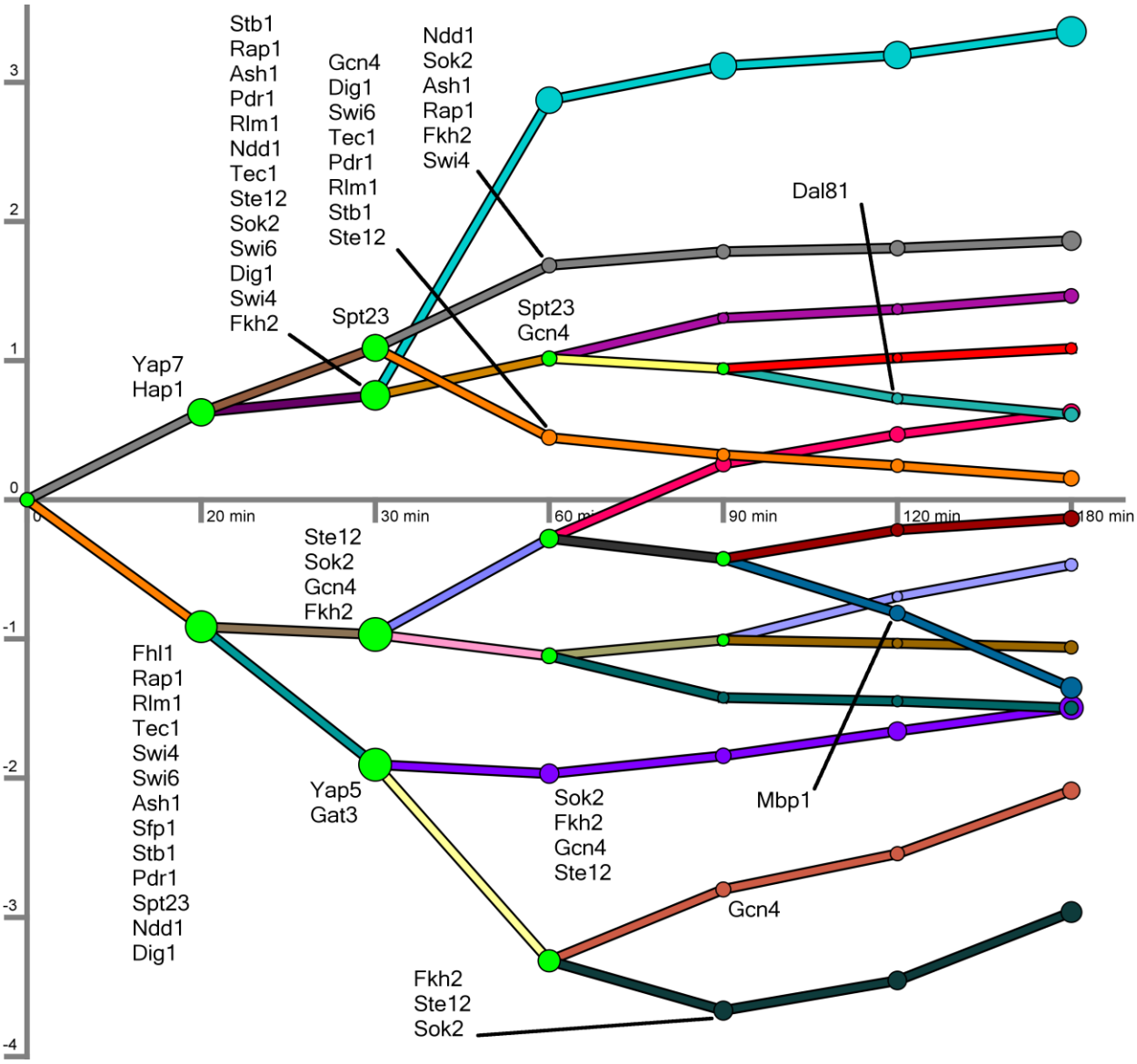


**Supplementary Figure S9. Rapamycin model regulatory paths.** The rapamycin response model contains 15 regulatory paths. Unlike the long osmotic stress model, the differentially expressed genes remain highly or lowly expressed after the initial shock for the duration of the experiments. TFs are shown only the first time they appear on a path.

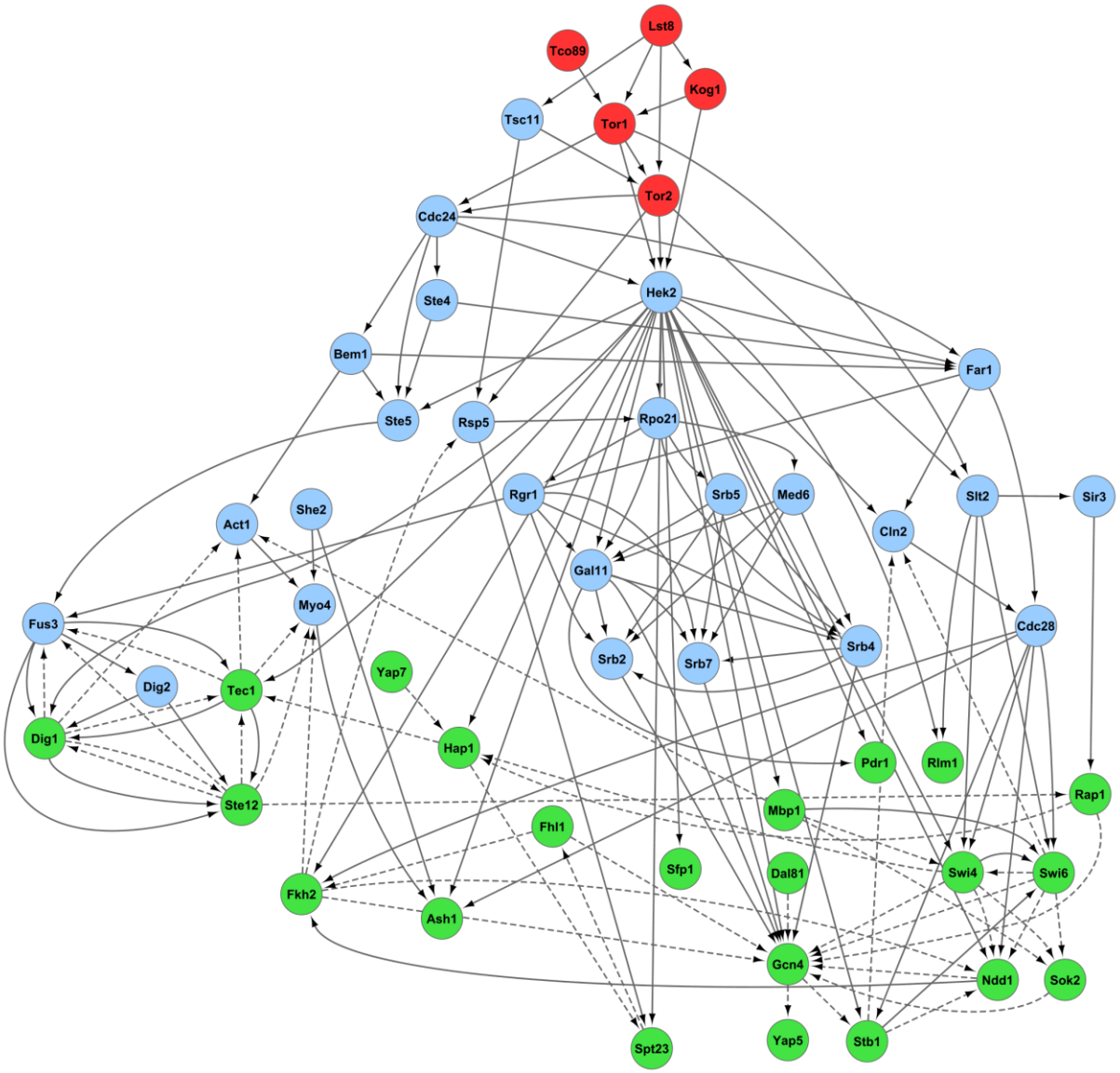


**Supplementary Figure S10. Rapamycin model signaling network.** The sources, signaling proteins, and active TFs in the rapamycin model are displayed. The TF Gat3 does not appear in the figure because it does not directly interact with other predicted pathway members. Rather, it is influenced by upstream proteins via paths containing other proteins that were not deemed to be core members of the response.

**Supplementary Table S8. TOR model targets.** The Zaman *et al* (Zaman et al. 2008) and SGD model columns indicate whether the predicted TF is a member of these TOR pathway representations. In the Xie *et al* column (Xie et al. 2005), the number of '-' symbols indicates the degree of rapamycin sensitivity, if any. The Hillenmeyer *et al* column provides the lowest p-value in multiple replicates of another rapamycin screen (Hillenmeyer et al. 2008). Each '-' in the Chan *et al* column indicates an order of magnitude decrease in rapamycin resistance (Chan et al. 2000). The rapamycin phenotype annotations were collected from SGD.

| Gene | ORF name | Zaman *et al* | SGD model | Xie *et al* | Hillenmeyer *et al* | Chan *et al* | Rapamycin phenotype | Literature |
|---|---|---|---|---|---|---|---|---|
| Ash1 | YKL185W | N | N | N/A | $2.69 \times 10^{-5}$ | N/A | Y | |
| Dal81 | YIR023W | N | N | N/A | $1.00 \times 10^{-20}$ | N/A | N | Dal81 was implicated as a TF active in rapamycin response (Bar-Joseph et al. 2003) based on evidence in (Scott et al. 2000). |
| Dig1 | YPL049C | N | N | N/A | $3.18 \times 10^{-6}$ | N/A | Y | |
| Fhl1 | YPR104C | N | N | N/A | N/A | N/A | N | The TOR pathway regulation of ribosomal protein transcription involves Fhl1 (Martin et al. 2004; Xiao and Grove 2009). |
| Fkh2 | YNL068C | N | N | N/A | $5.55 \times 10^{-17}$ | N/A | N | |
| Gcn4 | YEL009C | N | N | N/A | $4.18 \times 10^{-1}$ | N/A | N | Many Gcn4 targets are induced by rapamycin, and a subset of these requires Gcn4 for full induction (Natarajan et al. 2001). |
| Mbp1 | YDL056W | N | N | N/A | $1.88 \times 10^{-3}$ | N/A | Y | |
| Rap1 | YNL216W | N | N | N/A | N/A | N/A | N | Downstream TOR pathway transcriptional activity controlled |

| | | | | | | | | |
|---|---|---|---|---|---|---|---|---|
| | | | | | | | | by Hmo1 and Fhl1 appears to be dependent on Rap1 (Xiao and Grove 2009). |
| Rlm1 | YPL089C | N | N | N/A | $1.51 \times 10^{-3}$ | N/A | Y | The TORC1 complex is the primary target of caffeine, and Rlm1 is implicated in caffeine sensitivity (Truman et al. 2009). |
| Sfp1 | YLR403W | Y | N | N/A | $3.05 \times 10^{-2}$ | N/A | Y | |
| Sok2 | YMR016C | N | N | N/A | $3.29 \times 10^{-1}$ | N/A | N | Sok2 mutation reverses the negative effects of rapamycin on filamentous growth (Cutler et al. 2001). |
| Spt23 | YKL020C | N | N | N/A | $9.52 \times 10^{-5}$ | N/A | N | |
| Stb1 | YNL309W | N | N | N/A | N/A | N/A | N | Stb1 deletion leads to partial rapamycin resistance (Tsang et al. 2003). |
| Ste12 | YHR084W | N | N | - - | N/A | N/A | Y | |
| Swi4 | YER111C | N | N | N/A | $3.73 \times 10^{-2}$ | N/A | N | Swi4 is a member of the SBF transcription complex, which plays a role in caffeine-induced cell wall remodeling (Kuranda et al. 2006). |
| Swi6 | YLR182W | N | N | N/A | $8.12 \times 10^{-3}$ | - - - | N | Swi6 is a member of the SBF transcription complex, which plays a role in caffeine-induced cell wall remodeling (Kuranda et al. 2006). |
| Tec1 | YBR083W | N | N | N/A | $8.54 \times 10^{-2}$ | N/A | Y | Tec1 overexpression reverses the |

| | | | | | | | | |
|---|---|---|---|---|---|---|---|---|
| | | | | | | | | negative effects of rapamycin on filamentous growth (Cutler et al. 2001). |
| Gat3 | YLR013W | N | N | N/A | $3.28 \times 10^{-3}$ | N/A | N | |
| Hap1 | YLR256W | N | N | N/A | N/A | N/A | N | |
| Ndd1 | YOR372C | N | N | N/A | N/A | N/A | N | |
| Pdr1 | YGL013C | N | N | N/A | $1.00 \times 10^{-3}$ | N/A | N | |
| Yap5 | YIR018W | N | N | N/A | $4.56 \times 10^{-1}$ | N/A | N | |
| Yap7 | YOL028C | N | N | N/A | $2.45 \times 10^{-1}$ | N/A | N | |

SDREM identifies 25 additional proteins that connect TORC1 to the downstream TFs (Supplementary Fig. S9). Of these, 14 (56%) are present in the extended gold standard or were found to have possible links to the TOR pathway in a literature search (Supplementary Table S9). Altogether, the overlap between SDREM's TOR predictions and the extended gold standard is significant (p-value $2.55 \times 10^{-3}$ using Fisher's exact test). Therefore, even though very few predictions were present in the two canonical TOR models and many known TOR members were not recovered, SDREM accurately identifies an extended TOR pathway representation. The SDREM model includes many proteins that are traditionally primarily associated with other signaling pathways but are affected by rapamycin, for example Dig1, and explains how they may in fact be involved in the rapamycin response.

**Supplementary Table S9. TOR model internal nodes.** See Supplementary Table S8 for column descriptions.

| Gene | ORF name | Zaman *et al* | SGD model | Xie *et al* | Hillenmeyer *et al* | Chan *et al* | Rapamycin phenotype | Literature |
|---|---|---|---|---|---|---|---|---|
| Act1 | YFL039C | N | N | - - - - | N/A | N/A | Y | |
| Bem1 | YBR200W | N | N | N/A | $1.62 \times 10^{-2}$ | - - - | N | |
| Cdc28 | YBR160W | N | N | N/A | N/A | N/A | N | TORC1 mediates Cdc5, which activates Cdc28 (Nakashima et al. 2008). |
| Cln2 | YPL256C | N | N | N/A | $1.47 \times 10^{-8}$ | N/A | N | Rapamycin treatment reduces Cln2 levels (Zinzalla et al. 2007). |
| Fus3 | YBL016W | N | N | N/A | N/A | N/A | Y | |
| Gal11 | YOL051W | N | N | N/A | $3.01 \times 10^{-1}$ | N/A | Y | |
| Hek2 | YBL032W | N | N | N/A | $4.82 \times 10^{-9}$ | N/A | N | |
| Rsp5 | YER125W | N | N | N/A | N/A | N/A | N | Rsp5 deletion blocks the effects of rapamycin on Hxt1, a TOR signaling target (Schmelzle et al. 2004). |
| Sir3 | YLR442C | N | N | N/A | N/A | N/A | Y | |
| Slt2 | YHR030C | N | N | - - - | $1.82 \times 10^{-3}$ | - - - - | Y | |
| Srb2 | YHR041C | N | N | N/A | $7.73 \times 10^{-3}$ | - - | N | |
| Ste4 | YOR212W | N | N | N/A | N/A | N/A | N | Rapamycin effects have been shown to be Ste4-dependent (Zhu and Wang 2009). |
| Ste5 | YDR103W | N | N | N/A | N/A | N/A | N | Rapamycin effects have been shown to be Ste5-dependent (Zhu and Wang 2009). |
| Tsc11 | YER093C | N | Y | N/A | N/A | N/A | N | |
| Cdc24 | YAL041W | N | N | N/A | N/A | N/A | N | |
| Dig2 | YDR480W | N | N | N/A | $3.52 \times 10^{-1}$ | N/A | N | |
| Far1 | YJL157C | N | N | N/A | $8.82 \times 10^{-2}$ | N/A | N | |
| Med6 | YHR058C | N | N | N/A | N/A | N/A | N | |
| Myo4 | YAL029C | N | N | N/A | $2.54 \times 10^{-1}$ | N/A | N | |
| Rgr1 | YLR071C | N | N | N/A | N/A | N/A | N | |

| | | | | | | | | |
|---|---|---|---|---|---|---|---|---|
| Rpo21 | YDL140C | N | N | N/A | N/A | N/A | N | |
| She2 | YKL130C | N | N | N/A | $1.60 \times 10^{-2}$ | N/A | N | |
| Srb4 | YER022W | N | N | N/A | N/A | N/A | N | |
| Srb5 | YGR104C | N | N | N/A | $2.36 \times 10^{-1}$ | N/A | N | |
| Srb7 | YDR308C | N | N | N/A | N/A | N/A | N | |

***Arabidopsis thaliana* immune response model**

Although the gene expression measurements span nearly one week, the inferred regulatory paths in the SDREM model of *Arabidopsis* response to *Hyaloperonospora arabidopsidis* (*Hpa*) indicate that the transcriptional changes are sustained over this long period (Supplementary Fig. S11). Many of the predicted active TFs are active at numerous splits along the regulatory paths. We found that these TFs are very strongly connected to the *Hpa* effectors (the pathogen proteins used as the sources) in the signaling network and hence have strong activity priors. However, they bind relatively few genes on some of the regulatory paths so their high activity scores are primarily due to the strong priors (which are invariant across the different splits) as opposed to the behavior of their bound genes at each split. The signaling pathways in the SDREM model are shown in Supplementary Fig. S12, and Supplementary Table S10 provides the full model including the sources and SDREM predictions.

Mukhtar *et al* examined insertion mutants of 17 *Arabidopsis* proteins that are targeted by both *Hpa* and the *Pseudomonas syringae* bacterium (Mukhtar et al. 2011). Fifteen of these exhibited enhanced host susceptibility or resistance to infection by various *Hpa* isolates, and 6 of the validated proteins – APC8, AT3G27960, ATTCP15, CSN5A, LSU2, and TCP14 – were predicted by SDREM (p-value $7.29 \times 10^{-8}$, Fisher's exact test). Another 7 of SDREM's predictions – internal nodes HUB1, MOS6, and NIMIN1 as well as targets TGA2, TGA3,

WRKY53, and WRKY60 – were annotated as "defense response" proteins in Gene Ontology (Ashburner et al. 2000).

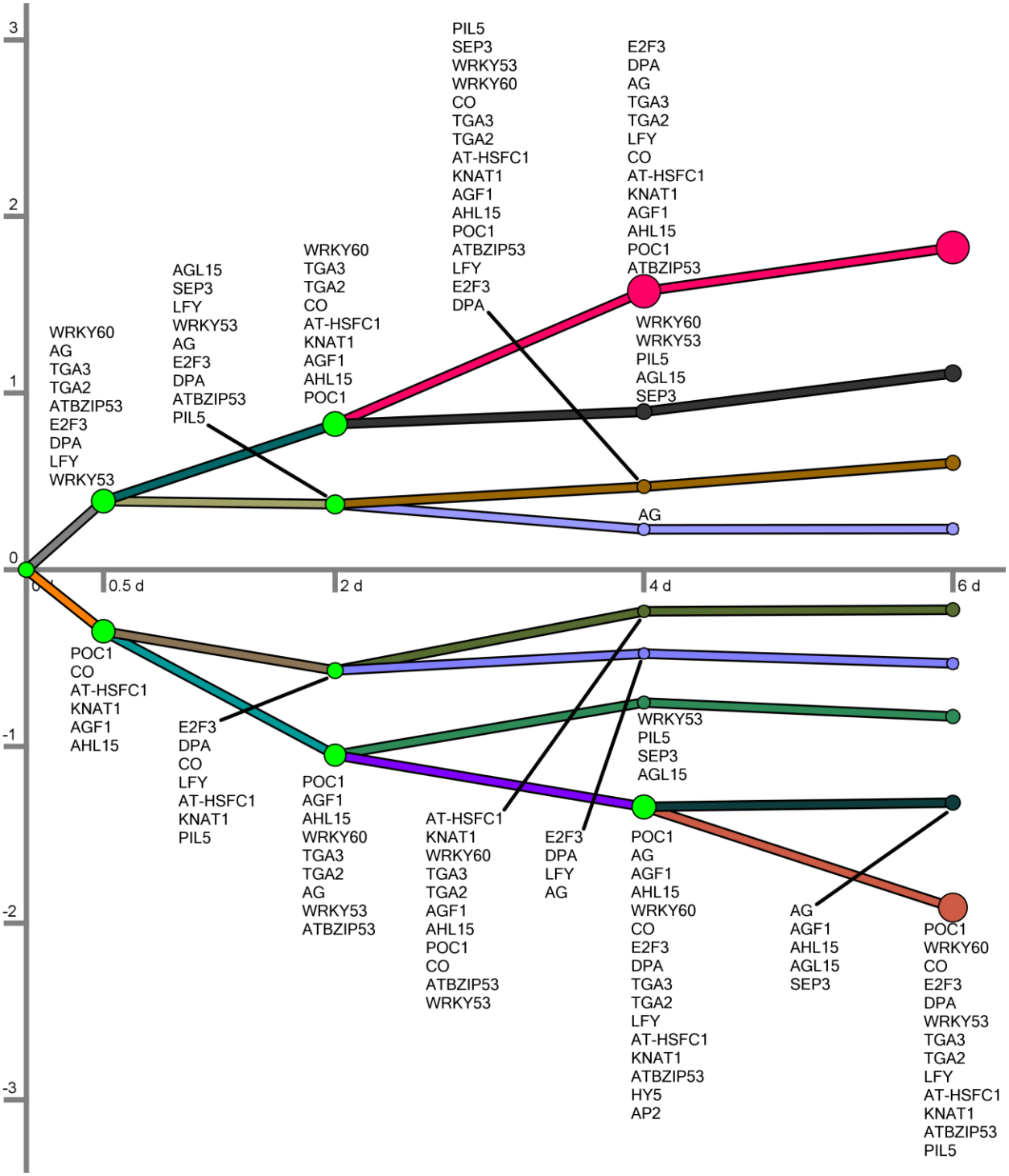


**Supplementary Figure S11.** ***Arabidopsis thaliana*** **regulatory paths.**

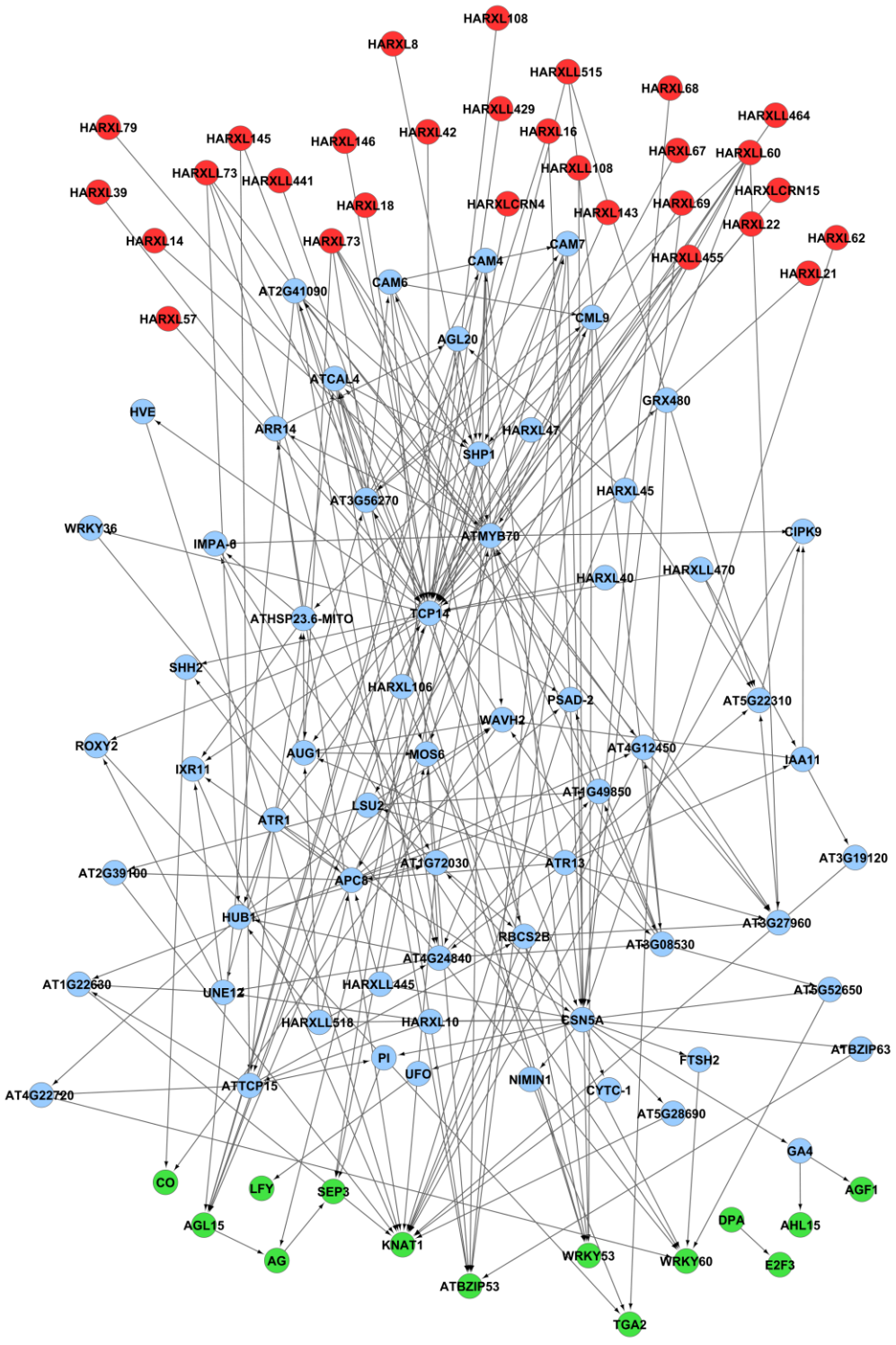


**Supplementary Figure S12. *Arabidopsis thaliana* signaling pathways.** The sources (red nodes) are *Hpa* effectors. The remaining proteins are predicted *Arabidopsis* immune responders.

**Supplementary Table S10. SDREM *Arabidopsis thaliana* immune response model.** The Role column designates whether the gene is a source (*Hpa* effector that was given as input), internal signaling node, or TF target. Some of the effectors that belong to the same family were grouped in the original data.

| Gene | Locus / id | Role |
|---|---|---|
| ATR1 family | ATR1_group | Source |
| ATR13 family | ATR13_group | Source |
| HARXL10 family | HARXL10_WACO9 | Source |
| HARXL106 family | HARXL106_group | Source |
| HARXL108 | HARXL108 | Source |
| HARXL11 | HARXL11 | Source |
| HARXL119 | HARXL119 | Source |
| HARXL12 | HARXL12 | Source |
| HARXL13 | HARXL13 | Source |
| HARXL14 | HARXL14 | Source |
| HARXL143 | HARXL143 | Source |
| HARXL144 | HARXL144 | Source |
| HARXL145 | HARXL145 | Source |
| HARXL146 | HARXL146 | Source |
| HARXL147 | HARXL147 | Source |
| HARXL148 | HARXL148 | Source |
| HARXL149 | HARXL149 | Source |
| HARXL15 | HARXL15 | Source |
| HARXL16 | HARXL16 | Source |
| HARXL17 family | HARXL17_WACO9 | Source |
| HARXL18 | HARXL18 | Source |
| HARXL21 | HARXL21 | Source |
| HARXL22 | HARXL22 | Source |
| HARXL23 | HARXL23 | Source |
| HARXL36 | HARXL36 | Source |
| HARXL39 | HARXL39 | Source |
| HARXL4 | HARXL4 | Source |
| HARXL40 family | HARXL40_group | Source |
| HARXL42 | HARXL42 | Source |
| HARXL44 | HARXL44 | Source |
| HARXL45 family | HARXL45_group | Source |
| HARXL47 family | HARXL47_group | Source |
| HARXL56 | HARXL56 | Source |

| | | |
|---|---|---|
| HARXL57 | HARXL57 | Source |
| HARXL59 | HARXL59 | Source |
| HARXL60 | HARXL60 | Source |
| HARXL62 | HARXL62 | Source |
| HARXL63 | HARXL63 | Source |
| HARXL64 | HARXL64 | Source |
| HARXL65 | HARXL65 | Source |
| HARXL67 | HARXL67 | Source |
| HARXL68 | HARXL68 | Source |
| HARXL69 | HARXL69 | Source |
| HARXL70 | HARXL70 | Source |
| HARXL72 | HARXL72 | Source |
| HARXL73 | HARXL73 | Source |
| HARXL74 | HARXL74 | Source |
| HARXL75 family | HARXL75_WACO9 | Source |
| HARXL76 family | HARXL76_WACO9 | Source |
| HARXL77 family | HARXL77_group | Source |
| HARXL78 family | HARXL78_group | Source |
| HARXL79 | HARXL79 | Source |
| HARXL8 | HARXL8 | Source |
| HARXL80 family | HARXL80_group | Source |
| HARXL89 | HARXL89 | Source |
| HARXLCRN15 | HARXLCRN15 | Source |
| HARXLCRN17 | HARXLCRN17 | Source |
| HARXLCRN4 | HARXLCRN4 | Source |
| HARXLL108 | HARXLL108 | Source |
| HARXLL148 | HARXLL148 | Source |
| HARXLL169 | HARXLL169 | Source |
| HARXLL429 | HARXLL429 | Source |
| HARXLL431 family | HARXLL431_WACO9 | Source |
| HARXLL437 | HARXLL437 | Source |
| HARXLL440 | HARXLL440 | Source |
| HARXLL441 | HARXLL441 | Source |
| HARXLL445 family | HARXLL445_group | Source |
| HARXLL446 | HARXLL446 | Source |
| HARXLL449 | HARXLL449 | Source |
| HARXLL455 | HARXLL455 | Source |
| HARXLL464 | HARXLL464 | Source |
| HARXLL468 | HARXLL468 | Source |
| HARXLL470 family | HARXLL470_WACO9 | Source |
| HARXLL480 | HARXLL480 | Source |

| | | |
|---|---|---|
| HARXLL492 | HARXLL492 | Source |
| HARXLL493 | HARXLL493 | Source |
| HARXLL495 | HARXLL495 | Source |
| HARXLL497 | HARXLL497 | Source |
| HARXLL515 | HARXLL515 | Source |
| HARXLL516 family | HARXLL516_WACO9 | Source |
| HARXLL517 family | HARXLL517_WACO9 | Source |
| HARXLL518 family | HARXLL518_WACO9 | Source |
| HARXLL519 family | HARXLL519_WACO9 | Source |
| HARXLL520 family | HARXLL520_WACO9 | Source |
| HARXLL60 | HARXLL60 | Source |
| HARXLL62_A | HARXLL62_A | Source |
| HARXLL62_B | HARXLL62_B | Source |
| HARXLL73 | HARXLL73 | Source |
| HARXLL73 family | HARXLL73_group | Source |
| HARXLL91 | HARXLL91 | Source |
| HARXLL94 | HARXLL94 | Source |
| AGL20 | AT2G45660 | Internal |
| APC8 | AT3G48150 | Internal |
| ARR14 | AT2G01760 | Internal |
| AT1G22630 | AT1G22630 | Internal |
| AT1G49850 | AT1G49850 | Internal |
| AT1G72030 | AT1G72030 | Internal |
| AT2G39100 | AT2G39100 | Internal |
| AT2G41090 | AT2G41090 | Internal |
| AT3G08530 | AT3G08530 | Internal |
| AT3G19120 | AT3G19120 | Internal |
| AT3G27960 | AT3G27960 | Internal |
| AT3G56270 | AT3G56270 | Internal |
| AT4G12450 | AT4G12450 | Internal |
| AT4G22720 | AT4G22720 | Internal |
| AT4G24840 | AT4G24840 | Internal |
| AT5G22310 | AT5G22310 | Internal |
| AT5G28690 | AT5G28690 | Internal |
| AT5G52650 | AT5G52650 | Internal |
| ATBZIP63 | AT5G28770 | Internal |
| ATCAL4 | AT2G41100 | Internal |
| ATHSP23.6-MITO | AT4G25200 | Internal |
| ATMYB70 | AT2G23290 | Internal |
| ATR1 | ATR1 | Internal |
| ATR13 | ATR13 | Internal |

| | | |
|---|---|---|
| ATTCP15 | AT1G69690 | Internal |
| AUG1 | AT2G41350 | Internal |
| CAM4 | AT1G66410 | Internal |
| CAM6 | AT5G21274 | Internal |
| CAM7 | AT3G43810 | Internal |
| CIPK9 | AT1G01140 | Internal |
| CML9 | AT3G51920 | Internal |
| CSN5A | AT1G22920 | Internal |
| CYTC-1 | AT1G22840 | Internal |
| FTSH2 | AT2G30950 | Internal |
| GA4 | AT1G15550 | Internal |
| GRX480 | AT1G28480 | Internal |
| HARXL10 | HARXL10 | Internal |
| HARXL106 | HARXL106 | Internal |
| HARXL40 | HARXL40 | Internal |
| HARXL45 | HARXL45 | Internal |
| HARXL47 | HARXL47 | Internal |
| HARXLL445 | HARXLL445 | Internal |
| HARXLL470 | HARXLL470 | Internal |
| HARXLL518 | HARXLL518 | Internal |
| HUB1 | AT2G44950 | Internal |
| HVE | AT2G02560 | Internal |
| IAA11 | AT4G28640 | Internal |
| IMPA-6 | AT1G02690 | Internal |
| IXR11 | AT1G62990 | Internal |
| LSU2 | AT5G24660 | Internal |
| MOS6 | AT4G02150 | Internal |
| NIMIN1 | AT1G02450 | Internal |
| PI | AT5G20240 | Internal |
| PSAD-2 | AT1G03130 | Internal |
| RBCS2B | AT5G38420 | Internal |
| ROXY2 | AT5G14070 | Internal |
| SHH2 | AT3G18380 | Internal |
| SHP1 | AT3G58780 | Internal |
| TCP14 | AT3G47620 | Internal |
| UFO | AT1G30950 | Internal |
| UNE12 | AT4G02590 | Internal |
| WAVH2 | AT5G65683 | Internal |
| WRKY36 | AT1G69810 | Internal |
| AG | AT4G18960 | Target |
| AGF1 | AT4G35390 | Target |

| | | |
|---|---|---|
| AGL15 | AT5G13790 | Target |
| AHL15 | AT3G55560 | Target |
| AP2 | AT4G36920 | Target |
| ATBZIP53 | AT3G62420 | Target |
| AT-HSFC1 | AT3G24520 | Target |
| CO | AT5G15840 | Target |
| DPA | AT5G02470 | Target |
| E2F3 | AT2G36010 | Target |
| HY5 | AT5G11260 | Target |
| KNAT1 | AT4G08150 | Target |
| LFY | AT5G61850 | Target |
| PIL5 | AT2G20180 | Target |
| POC1 | AT1G09530 | Target |
| SEP3 | AT1G24260 | Target |
| TGA2 | AT5G06950 | Target |
| TGA3 | AT1G22070 | Target |
| WRKY53 | AT4G23810 | Target |
| WRKY60 | AT2G25000 | Target |

**Physical Network Models and ResponseNet comparison**

PNM predicts a very large set of proteins, 445 for the short expression data and 309 for the long expression data. Even though it predicts over 6 times more proteins than SDREM in both cases, it recovers only 2 or 3 more gold standard proteins than SDREM, resulting in less significant overlaps. The noteworthy omission of Hog1 in the PNM network constructed with the long expression data and insignificant overlap between the predicted TFs and gold standard TFs indicate the HOG pathway is not well-represented even in the large predicted network. In the main text, we anecdotally demonstrated 7 interactions from the HOG pathway that SDREM oriented correctly in the short model. Of these 7, PNM correctly orients the edges Ste50→Ste11, Sho1→Pbs2, Pbs2→Hog1, and Hog1→Sko1 but does not include the edges Sho1→Ste11, Ste11→Pbs2, or Hog1→Hot1 in its pathways. Although this sample is far too small to draw any broad conclusions, these results may suggest that PNM can correctly orient critical HOG

pathway edges but struggles to identify the relevant nodes and interactions relative to SDREM (Table 1).

When run with the default settings, ResponseNet's capping parameter is set to 0.7, which controls the maximum edge weight in the network. The majority of the edge weights in our interaction network are $\geq 0.7$ so this leads to a network where most of the edges have the same maximum weight of 0.7. Consequently, ResponseNet struggles to predict internal signaling nodes in this setting and includes only 4 such proteins in its network. Hog1 is not among those 4 proteins, and the large set of predicted TFs does not significantly overlap the HOG gold standard TFs (Table 1).

Therefore, we varied the capping parameter from 0.6 (the smallest value tested in Yeger-Lotem *et al* (Yeger-Lotem et al. 2009)) to 1.0 (the maximum possible value) and the gamma parameter, which generally controls the network size, from 5 to 20 (the recommended range) and reran ResponseNet on the short expression data. We found that the internal node predictions were significantly better under different settings. For example, when gamma is 10 and capping is 0.9, 4 of the 8 predicted signaling proteins are in the HOG pathway (p-value $5.99 \times 10^{-8}$), including Hog1.

Surprisingly, the TF predictions are independent of the choice of gamma and are affected only by the capping parameter (Supplementary Table S11). In all cases, ResponseNet recovers between 0 and 2 known HOG pathway TFs, and the overlaps with the HOG TFs are insignificant. One possible explanation is that ResponseNet cannot analyze gene expression dynamics, which

impairs its ability to recover the HOG TFs. SDREM works directly with the temporal expression values, which enables it to identify time points when a subset of a TF's bound genes are differentially expressed (diverging from genes not bound by the TF). These patterns may not emerge in a static dataset.

**Supplementary Table S11. ResponseNet TF predictions under various parameter settings.** Gamma (default value 10) and capping (default value 0.7) are the ResponseNet parameters that were varied.

| Gamma | Capping | Predicted TFs | Gold standard TFs | TF overlap | TF significance |
|---|---|---|---|---|---|
| 5 | 0.6 | 59 | 7 | 2 | 0.655 |
| 5 | 0.7 | 57 | 7 | 2 | 0.632 |
| 5 | 0.8 | 5 | 7 | 1 | 0.162 |
| 5 | 0.9 | 5 | 7 | 1 | 0.162 |
| 5 | 1 | 6 | 7 | 0 | 1.000 |
| 10 | 0.6 | 59 | 7 | 2 | 0.655 |
| 10 | 0.7 | 57 | 7 | 2 | 0.632 |
| 10 | 0.8 | 5 | 7 | 1 | 0.162 |
| 10 | 0.9 | 5 | 7 | 1 | 0.162 |
| 10 | 1 | 6 | 7 | 0 | 1.000 |
| 15 | 0.6 | 59 | 7 | 2 | 0.655 |
| 15 | 0.7 | 57 | 7 | 2 | 0.632 |
| 15 | 0.8 | 5 | 7 | 1 | 0.162 |
| 15 | 0.9 | 5 | 7 | 1 | 0.162 |
| 15 | 1 | 6 | 7 | 0 | 1.000 |
| 20 | 0.6 | 59 | 7 | 2 | 0.655 |
| 20 | 0.7 | 57 | 7 | 2 | 0.632 |
| 20 | 0.8 | 5 | 7 | 1 | 0.162 |
| 20 | 0.9 | 5 | 7 | 1 | 0.162 |
| 20 | 1 | 6 | 7 | 0 | 1.000 |

**GeneReg comparison**

GeneReg is an algorithm that uses time-lagged linear regression to extract potential regulatory relationships from time series gene expression data (Huang et al. 2010). We selected GeneReg

in particular because similar approaches that rely on time-lagged correlation (Schmitt et al. 2004; Balasubramaniyan et al. 2005) or time-lagged mutual information (Zoppoli et al. 2010) either do not make their software available (Schmitt et al. 2004; Balasubramaniyan et al. 2005) or do not scale to handle thousands of genes information (Zoppoli et al. 2010). We ran GeneReg on the long expression dataset since the temporal patterns in this dataset, which captures the response and recovery, should be easier for a time-lagged method to detect. However, when we evaluated the TFs that GeneReg predicted to be most active in the stress response at several thresholds, its predictions did not significantly overlap with the HOG gold standard TFs (Supplementary Table S12). Note that some of these top-ranked TFs were in the osmotic stress screens even though they are not gold standard TFs, and Msn4 ranked just outside of the top 28 TFs. Even in the best case, algorithms that rely on expression data alone can only recover TFs that are differentially expressed. In contrast, we found evidence that only a handful of TFs are transcriptionally activated in the long model, and in the short model even fewer HOG TFs are differentially expressed, which emphasizes the benefits of jointly modeling the upstream interaction networks and the dynamic expression data like SDREM.

**Supplementary Table S12. Evaluation of GeneReg TF predictions.** At various thresholds, the top-ranked TFs from GeneReg do not significantly overlap with the HOG TFs. The SDREM TF predictions (28 targets and 6 TFs in the set of internal nodes) from the long model are shown for comparison.

| **Algorithm** | SDREM | GeneReg | GeneReg | GeneReg |
|---|---|---|---|---|
| **Predicted TFs** | 34 | 10 | 28 | 46 |
| **Gold standard TFs** | 7 | 7 | 7 | 7 |
| **TF overlap** | 4 | 1 | 2 | 3 |
| **TF significance** | 0.0161 | 0.302 | 0.249 | 0.194 |

**Parameter selection and robustness**

Whenever possible, SDREM's parameters were selected in accordance with existing biological data or computational approaches. We used condition-specific osmotic stress data to obtain an estimate for the active TF influence parameter, which represents the portion of bound genes that are expected to be affected by an active TF. The TFs Hot1 and Sko1 are the two HOG pathway TFs for which we have condition-specific binding data (Capaldi et al. 2008), and both are known to be active in the osmotic stress response. 79% of the genes bound by Hot1 are differentially expressed in both the short osmotic stress expression data and the long expression data. Likewise, 79% of genes bound by Sko1 are affected in the short expression data and 68% in the long expression dataset. Therefore, we set this parameter's default value to 80%.

Several parameters such as the path length, PPI edge weight threshold, and number of top paths used for scoring were selected from a detailed analysis we performed on yeast PPI networks (Gitter et al. 2011). We showed that using a path length of 5 is a reasonable compromise between coverage and computational complexity, that edges with a weight of less than 0.6 are generally low-confidence interactions that have not been reported multiple times or detected using a high-confidence experimental technology and are thus less beneficial for pathway reconstruction, and that by focusing on the smaller set of the top 100 paths we can achieve better precision and recall compared to using more paths. In this previous study, the number of targets in the network was fixed, which suggested using a fixed threshold for the number of top paths. The number of paths considered by SDREM is equal to 5 times the number of targets instead of the fixed value of 100 to account for the fluctuating number of targets over all iterations. In the short model, this flexibility results in using between 95 and 140 top paths.

The protein-DNA edge weights (Supplementary Table S19) are motivated by the ResponseNet (Yeger-Lotem et al. 2009) and PPI network weighting schemes (Supplementary Methods). In Supplementary Materials of (Hillenmeyer et al. 2008), the authors recommend a p-value cutoff of $10^{-5}$ to control for multiple hypothesis testing across genes that are sensitive in any of the 178 conditions tested in the homozygous collection. However, because we are only interested in deletion strains that exhibit a fitness defect in one specific condition, we used a less stringent threshold of $10^{-4}$.

The differential expression thresholds differ for the short and long osmotic stress expression datasets due to disparities in the respective experimental frameworks. The two studies use different microarrays, osmostic stresses, sampling times, etc. (Gasch et al. 2000; Romero-Santacreu et al. 2009) leading to expression profiles that are not directly comparable. A lower differential expression threshold was used for the long osmotic stress expression data because this dataset exhibited lower magnitude fold changes. Using a lower expression threshold enabled us to analyze roughly the same number of genes in both osmotic stress expression datasets. Specifically, a $\log_2$ fold change threshold of 1 was used for the short osmotic stress data and 0.5 was used for the long expression data instead.

The activity score and node score thresholds were selected arbitrarily, but were found to yield good false positive rates. For the short model the target TF false positive rate is 13.3% and the internal node false positive rate is 0.6%. For the long model the target TF false positive rate is 21.2% and the internal node false positive rate is 0.3%. If we use both the HOG gold standard

and osmotic stress screens to define the positive and negative genes, the false positive rates are nearly identical.

For those parameters that could not be directly estimated from biological data, we made an initial choice of value based on our intuition of the algorithm's behavior. We then tested the robustness of this selection to small fluctuations in the parameter value (where robustness is measured in terms of the overlap in the outcomes between different parameter values), following the approach of (Kim et al. 2011). These parameters were consistent across all SDREM runs and are suitable for analysis of other conditions or organisms.

Supplementary Table S13 describes the 8 parameters that were varied during the robustness testing, all of which was performed using the short osmotic stress expression data. In addition to the 2 runs per parameter (using a lower/higher value than the default), we ran SDREM with an unweighted version of our protein-DNA interaction network to observe whether our weighting scheme enhanced SDREM's predictions. The topology of this unweighted network was identical to the original protein-DNA interaction network, but the weights were uniformly set to 1. The PPI edge weights were not changed because their weights have been justified previously (Gitter et al. 2011).

Although varying these parameters does have an effect on the SDREM output, the core of the predicted network remains the same. Nearly all of the new runs generate fewer predictions than the baseline run, but in the majority of the runs over 90% of the new predictions are also found in the baseline predictions (Supplementary Table S14). The notable exception is the set of

predictions from the unweighted protein-DNA interaction network, which has a greater effect than varying the algorithm's parameters. Only 25 of the 58 baseline short model predictions also appear in this run, lower than any of the overlaps obtained when only the parameters are varied. Supplementary Fig. S13 shows that out of the 58 proteins in the baseline short model, 31% are still predicted in all 16 runs where a parameter is varied and 79% are predicted in at least half of the runs. In contrast, the majority (56%) of the proteins that are predicted only when the parameters are varied appear in the output of a single run.

When varying the parameters, the overlap between SDREM's predictions and the HOG gold standard is significant in all cases and comparable to the overlap obtained when using the original parameters (Supplementary Tables S15 and S16). However, once again we observe that the run that uses the unweighted network is an outlier and performs markedly worse than the baseline prediction. Only 6 signaling proteins are predicted, and Hog1 is not among them, confirming that the protein-DNA edge weights we assigned improve predictive capabilities.

**Supplementary Table S13. Parameters perturbed for robustness testing.** In addition to the protein-DNA network weight, the 8 parameters below were varied for robustness testing. The baseline run uses the default value for all parameters.

| Run name | Parameter being varied | Default value | New value |
|---|---|---|---|
| baseline | None | | |
| active.tf.influence.0.7 | Percent of bound genes that are influenced by a TF that is active in the stress response | 80% | 70% |
| active.tf.influence.0.9 | Percent of bound genes that are influenced by a TF that is active in the stress response | 80% | 90% |
| dist.tfs.25 | Number of TFs used to build random activity score distribution | 50 | 25 |
| dist.tfs.100 | Number of TFs used to build random activity score distribution | 50 | 100 |
| dist.thresh.0.4 | Percentile in the random activity score distribution that real TF scores must exceed | $50^{th}$ | $40^{th}$ |
| dist.thresh.0.6 | Percentile in the random activity score distribution that real TF scores must exceed | $50^{th}$ | $60^{th}$ |
| min.prior.0.005 | Minimum activity prior allowed | 0.01 | 0.005 |
| min.prior.0.05 | Minimum activity prior allowed | 0.01 | 0.05 |
| node.thresh.0.005 | Node score threshold | 0.01 | 0.005 |
| node.thresh.0.05 | Node score threshold | 0.01 | 0.05 |
| random.target.ratio.0.5 | Number of random targets added to network during target scoring per real target | 1 | 0.5 |
| random.target.ratio.2 | Number of random targets added to network during target scoring per real target | 1 | 2 |
| target.thresh.0.7 | Target score distribution threshold | 0.8 | 0.7 |
| target.thresh.0.9 | Target score distribution threshold | 0.8 | 0.9 |
| top.paths.100 | Number of top-ranked paths used to calculate target and node scores in the network | 5 times number of targets | 100 |
| top.paths.1000 | Number of top-ranked paths used to calculate target and node scores in the network | 5 times number of targets | 1000 |
| pdi.no.weight | Protein-DNA interaction network edge weights | See text | See text |

**Supplementary Table S14. Baseline overlap during perturbation testing.** The number of proteins predicted by the baseline model and the runs in which a single parameter was varied. The five sources are present in all models and are not included in the counts. Overlap percentages are calculated with respect to the baseline ('Baseline overlap') and the robustness testing run ('Run overlap').

| Run name | Baseline predictions | Run predictions | Overlap | Baseline overlap | Run overlap |
|---|---|---|---|---|---|
| active.tf.influence.0.7 | 58 | 46 | 41 | 71% | 89% |
| active.tf.influence.0.9 | 58 | 28 | 28 | 48% | 100% |
| dist.tfs.25 | 58 | 41 | 36 | 62% | 88% |
| dist.tfs.100 | 58 | 52 | 41 | 71% | 79% |
| dist.thresh.0.4 | 58 | 53 | 49 | 84% | 92% |
| dist.thresh.0.6 | 58 | 36 | 36 | 62% | 100% |
| min.prior.0.005 | 58 | 51 | 47 | 81% | 92% |
| min.prior.0.05 | 58 | 50 | 47 | 81% | 94% |
| node.thresh.0.005 | 58 | 57 | 55 | 95% | 96% |
| node.thresh.0.05 | 58 | 39 | 32 | 55% | 82% |
| random.target.ratio.0.5 | 58 | 58 | 55 | 95% | 95% |
| random.target.ratio.2 | 58 | 52 | 49 | 84% | 94% |
| target.thresh.0.7 | 58 | 58 | 55 | 95% | 95% |
| target.thresh.0.9 | 58 | 42 | 41 | 71% | 98% |
| top.paths.100 | 58 | 53 | 49 | 84% | 92% |
| top.paths.1000 | 58 | 68 | 45 | 78% | 66% |
| pdi.no.weight | 58 | 35 | 25 | 43% | 71% |

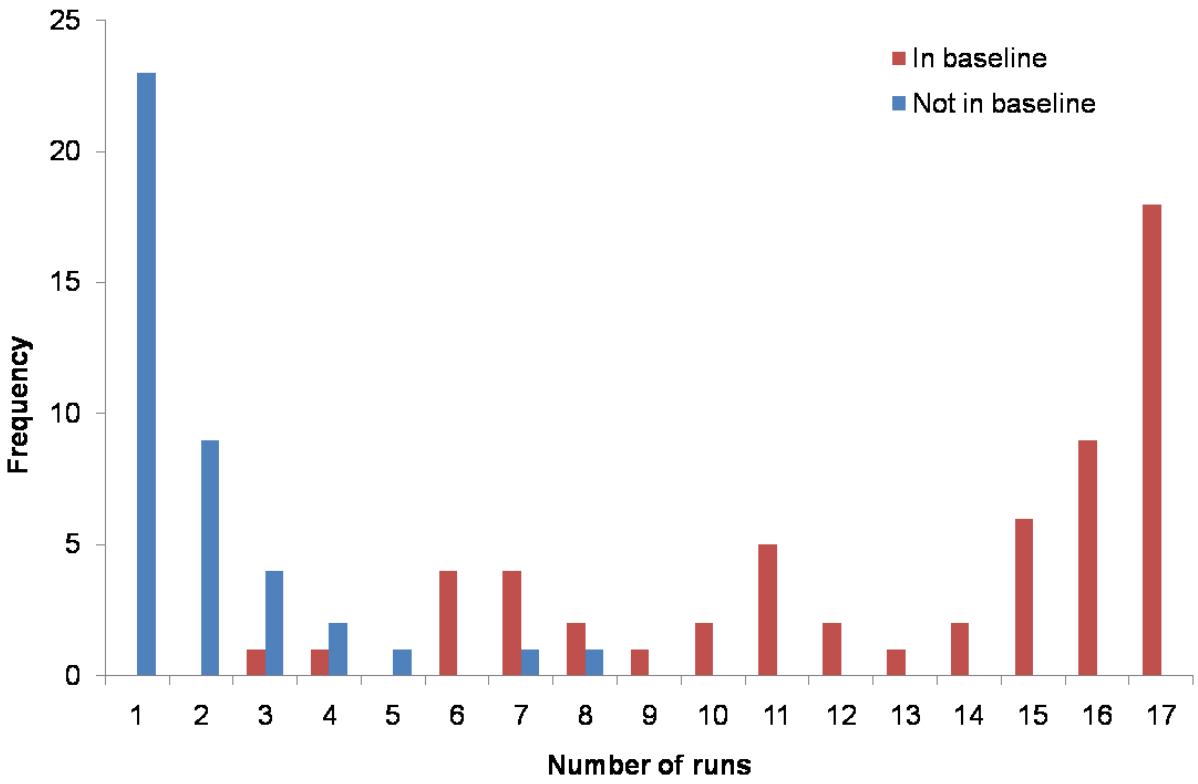


**Supplementary Figure S13. Histogram of the number of occurrences of each protein across all perturbation testing.** The number of runs specifies how many models include a particular protein. The frequency provides the number of proteins that fall into each bin. For example, 23 proteins are predicted in only a single run. The 'pdi.no.weight' run is not included in the counts. The five sources appear in all models and are also not counted.

**Supplementary Table S15. Robustness testing signaling protein overlap significance.** The significance of the overlap between the HOG gold standard signaling proteins (those that are not sources or TFs) and signaling proteins in the SDREM models. The total predictions include the signaling proteins and TFs, but not the five sources.

| Run name | Total predictions | Predicts Hog1 | Predicted signaling | Gold standard signaling | Signaling overlap | Signaling significance |
|---|---|---|---|---|---|---|
| baseline | 58 | Y | 30 | 30 | 6 | $1.11 \times 10^{-8}$ |
| active.tf.influence.0.7 | 46 | Y | 18 | 30 | 6 | $3.65 \times 10^{-10}$ |
| active.tf.influence.0.9 | 28 | Y | 11 | 30 | 4 | $2.79 \times 10^{-7}$ |
| dist.tfs.25 | 41 | Y | 22 | 30 | 6 | $1.44 \times 10^{-9}$ |
| dist.tfs.100 | 52 | Y | 16 | 30 | 5 | $1.80 \times 10^{-8}$ |
| dist.thresh.0.4 | 53 | Y | 21 | 30 | 6 | $1.05 \times 10^{-9}$ |
| dist.thresh.0.6 | 36 | Y | 17 | 30 | 5 | $2.55 \times 10^{-8}$ |
| min.prior.0.005 | 51 | Y | 21 | 30 | 6 | $1.05 \times 10^{-9}$ |
| min.prior.0.05 | 50 | Y | 22 | 30 | 6 | $1.44 \times 10^{-9}$ |
| node.thresh.0.005 | 57 | Y | 30 | 30 | 6 | $1.11 \times 10^{-8}$ |
| node.thresh.0.05 | 39 | Y | 11 | 30 | 4 | $2.79 \times 10^{-7}$ |
| random.target.ratio.0.5 | 58 | Y | 31 | 30 | 6 | $1.37 \times 10^{-8}$ |
| random.target.ratio.2 | 52 | Y | 21 | 30 | 6 | $1.05 \times 10^{-9}$ |
| target.thresh.0.7 | 58 | Y | 32 | 30 | 6 | $1.68 \times 10^{-8}$ |
| target.thresh.0.9 | 42 | Y | 20 | 30 | 5 | $6.30 \times 10^{-8}$ |
| top.paths.100 | 53 | Y | 29 | 30 | 6 | $8.94 \times 10^{-9}$ |
| top.paths.1000 | 68 | Y | 28 | 30 | 8 | $1.19 \times 10^{-12}$ |
| pdi.no.weight | 35 | N | 6 | 30 | 2 | $4.68 \times 10^{-4}$ |

**Supplementary Table S16. Robustness testing TF overlap significance.** The significance of the overlap between the HOG gold standard TFs and the SDREM model TFs. The total predictions include the signaling proteins and TFs, but not the five sources.

| Run name | Total predictions | Predicted TFs | Gold standard TFs | TF overlap | TF significance |
|---|---|---|---|---|---|
| baseline | 58 | 28 | 7 | 4 | 0.008 |
| active.tf.influence.0.7 | 46 | 28 | 7 | 4 | 0.008 |
| active.tf.influence.0.9 | 28 | 17 | 7 | 4 | 0.001 |
| dist.tfs.25 | 41 | 19 | 7 | 4 | 0.002 |
| dist.tfs.100 | 52 | 36 | 7 | 4 | 0.020 |
| dist.thresh.0.4 | 53 | 32 | 7 | 5 | 0.001 |
| dist.thresh.0.6 | 36 | 19 | 7 | 4 | 0.002 |
| min.prior.0.005 | 51 | 30 | 7 | 4 | 0.010 |
| min.prior.0.05 | 50 | 28 | 7 | 4 | 0.008 |
| node.thresh.0.005 | 57 | 27 | 7 | 4 | 0.007 |
| node.thresh.0.05 | 39 | 28 | 7 | 4 | 0.008 |
| random.target.ratio.0.5 | 58 | 27 | 7 | 4 | 0.007 |
| random.target.ratio.2 | 52 | 31 | 7 | 5 | 0.001 |
| target.thresh.0.7 | 58 | 26 | 7 | 4 | 0.006 |
| target.thresh.0.9 | 42 | 22 | 7 | 4 | 0.003 |
| top.paths.100 | 53 | 24 | 7 | 4 | 0.004 |
| top.paths.1000 | 68 | 40 | 7 | 5 | 0.004 |
| pdi.no.weight | 35 | 29 | 7 | 5 | 0.001 |

**Convergence properties**

Supplementary Tables S17 and S18 depict how the predicted TFs and internal nodes change over the 10 iterations. The long model best demonstrates how SDREM converges in practice (Supplementary Table S18). In the final 3 iterations, the same 51 proteins are predicted. The short model nearly converges after 10 iterations but is slightly less stable than the long model. Of the 58 predictions made in the final iteration, 54 are also predicted at the preceding iteration.

There is no single iteration that yields the most significant overlaps across all three metrics (gold standard signaling proteins, gold standard TFs, and gold standard with screens) for either model. When considering the osmotic stress screens, iteration 2 is best for the short model and iteration

1 is best for the long model. However, the long model in particular exhibits improvement over time with respect to the gold standard, and the long model TFs overlap most strongly with the gold standard at the final iteration. This highlights the reason we do not stop after only a few iterations. Initially, many of the predicted TFs are not connected to the upstream signaling pathways and some of the predicted signaling nodes are isolated from the core pathways. Because our goal is to recover interpretable models that may suggest mechanistic explanations of how each predicted protein is involved in the response (e.g. how a TF is activated), we iterate and prune predictions that are not jointly supported by the signaling pathways and transcriptional dynamics. Consequently, SDREM tends to predict fewer proteins as the iterations proceed, especially fewer TFs.

**Supplementary Table S17. Short model convergence.** The table shows the number of predictions made at each iteration of SDREM when run on the short osmotic stress expression data and the overlaps with the osmotic stress evidence. The HOG gold standard was used to evaluate the TFs and internal predictions individually and the combined osmotic stress evidence (HOG pathway members and osmotic stress screen hits) was used to evaluate the TFs and internal nodes together.

| **Iteration** | 1 | 2 | 3 | 4 | 5 | 6 | 7 | 8 | 9 | 10 |
|---|---|---|---|---|---|---|---|---|---|---|
| **Total predictions** | 69 | 46 | 44 | 59 | 51 | 49 | 49 | 46 | 57 | 58 |
| **Predicted internal** | 29 | 17 | 16 | 21 | 19 | 21 | 19 | 18 | 29 | 30 |
| **Gold standard internal** | 30 | 30 | 30 | 30 | 30 | 30 | 30 | 30 | 30 | 30 |
| **Internal overlap** | 6 | 6 | 6 | 6 | 6 | 6 | 6 | 6 | 5 | 6 |
| **Internal significance** | $8.94 \times 10^{-9}$ | $2.44 \times 10^{-10}$ | $1.59 \times 10^{-10}$ | $1.05 \times 10^{-9}$ | $5.31 \times 10^{-10}$ | $1.05 \times 10^{-9}$ | $5.31 \times 10^{-10}$ | $3.65 \times 10^{-10}$ | $4.66 \times 10^{-7}$ | $1.11 \times 10^{-8}$ |
| **Predicted TFs** | 40 | 29 | 28 | 38 | 32 | 28 | 30 | 28 | 28 | 28 |
| **Gold standard TFs** | 7 | 7 | 7 | 7 | 7 | 7 | 7 | 7 | 7 | 7 |
| **TF overlap** | 5 | 5 | 5 | 5 | 5 | 5 | 4 | 5 | 4 | 4 |
| **TF significance** | 0.00368 | $7.37 \times 10^{-4}$ | $6.16 \times 10^{-4}$ | 0.00286 | 0.00122 | $6.16 \times 10^{-4}$ | 0.0100 | $6.16 \times 10^{-4}$ | 0.00770 | 0.00770 |
| **Gold standard or screen hit** | 1167 | 1167 | 1167 | 1167 | 1167 | 1167 | 1167 | 1167 | 1167 | 1167 |
| **Combined overlap** | 28 | 21 | 19 | 23 | 22 | 21 | 20 | 19 | 20 | 21 |
| **Combined significance** | $1.85 \times 10^{-4}$ | $1.67 \times 10^{-4}$ | $8.00 \times 10^{-4}$ | 0.00132 | $3.21 \times 10^{-4}$ | $4.87 \times 10^{-4}$ | 0.00138 | 0.001529 | 0.0105 | 0.00588 |

**Supplementary Table S18. Long model convergence.** The table shows the number of predictions made at each iteration of SDREM when run on the long osmotic stress expression data and the overlaps with the osmotic stress evidence. The HOG gold standard was used to evaluate the TFs and internal predictions individually and the combined osmotic stress evidence (HOG pathway members and osmotic stress screen hits) was used to evaluate the TFs and internal nodes together.

| **Iteration** | 1 | 2 | 3 | 4 | 5 | 6 | 7 | 8 | 9 | 10 |
|---|---|---|---|---|---|---|---|---|---|---|
| **Total predictions** | 92 | 66 | 64 | 59 | 55 | 55 | 54 | 51 | 51 | 51 |
| **Predicted internal** | 29 | 18 | 20 | 19 | 19 | 19 | 19 | 17 | 17 | 17 |
| **Gold standard internal** | 30 | 30 | 30 | 30 | 30 | 30 | 30 | 30 | 30 | 30 |
| **Internal overlap** | 6 | 6 | 6 | 6 | 6 | 6 | 5 | 5 | 5 | 5 |
| **Internal significance** | $8.94 \times 10^{-9}$ | $3.65 \times 10^{-10}$ | $7.55 \times 10^{-10}$ | $5.31 \times 10^{-10}$ | $5.31 \times 10^{-10}$ | $5.31 \times 10^{-10}$ | $4.75 \times 10^{-8}$ | $2.55 \times 10^{-8}$ | $2.55 \times 10^{-8}$ | $2.55 \times 10^{-8}$ |
| **Predicted TFs** | 63 | 48 | 44 | 40 | 36 | 36 | 35 | 34 | 34 | 34 |
| **Gold standard TFs** | 7 | 7 | 7 | 7 | 7 | 7 | 7 | 7 | 7 | 7 |
| **TF overlap** | 4 | 4 | 4 | 4 | 4 | 4 | 4 | 4 | 4 | 4 |
| **TF significance** | 0.136 | 0.0555 | 0.0410 | 0.0292 | 0.0199 | 0.0199 | 0.0179 | 0.0161 | 0.0161 | 0.0161 |
| **Gold standard or screen hit** | 1167 | 1167 | 1167 | 1167 | 1167 | 1167 | 1167 | 1167 | 1167 | 1167 |
| **Combined overlap** | 31 | 21 | 19 | 19 | 18 | 18 | 17 | 17 | 17 | 17 |
| **Combined significance** | 0.00340 | 0.0279 | 0.0678 | 0.0314 | 0.0304 | 0.0304 | 0.0495 | 0.0292 | 0.0292 | 0.0292 |

## Supplementary Methods

### DREM modification details

At each split in the regulatory paths in the SDREM model, an activity score is calculated for all TFs. The score at a particular bifurcation event *e* is the likelihood ratio

$$score(t,e) = \frac{P(a=1 \mid G_t)}{P(a=0 \mid G_t)}$$

where *a* reflects whether the TF $t$ is active at this split and $G_t$ represents the expression profiles of the set of genes bound by *t* that are on the path into the split *e*. By applying Bayes rule and assuming that the expression profiles of bound genes are independent (a simplifying assumption that is unlikely to be true in real data) we obtain

$$\begin{aligned}\frac{P(a=1 \mid G_t)}{P(a=0 \mid G_t)} &= \frac{\frac{P(G_t \mid a=1)P(a=1)}{P(G_t)}}{\frac{P(G_t \mid a=0)P(a=0)}{P(G_t)}} \\ &= \frac{P(G_t \mid a=1)P(a=1)}{P(G_t \mid a=0)P(a=0)} \\ &= \frac{\left(\prod_{g_i \in G_t} P(g_i \mid a=1)\right)P(a=1)}{\left(\prod_{g_i \in G_t} P(g_i \mid a=0)\right)P(a=0)}\end{aligned}$$

Initially, we place a uniform prior on TF activity such that $P(a=1) = P(a=0) = 0.5$. In subsequent iterations, the prior is influenced by the network orientation such that TFs that are well-connected in the network have a larger prior. Specifically, the new prior of a well-connected TF is the average of 1.0 and the TF's prior at the previous iteration. Poorly connected TFs have their prior reduced but not beyond the minimum prior of 0.01.

To estimate the remaining probabilities, the set of bound genes $G_t$ is divided into two sets: those genes that are assigned to the primary path out of the split ($g_i = 1$) and those assigned to the secondary path(s) out of the split ($g_i = 0$). The set of genes assigned to the primary path is denoted $G_P$ and the set of genes on the secondary path is $G_S$. The primary path is the path out of the split followed by the majority of genes bound by the TF. In the case of a tie, the path with the fewest genes (regulated by any TF, not just *t*) that is involved in the tie becomes the primary path. All other paths out of the split are designated secondary paths and are considered as a single group. There will always be at least one secondary path because the TF activity score is only calculated at nodes in the model that have two or more children. After splitting genes by the path they take, the score becomes

$$\frac{\left(\prod_{g_i \in G_t} P(g_i \mid a=1)\right)P(a=1)}{\left(\prod_{g_i \in G_t} P(g_i \mid a=0)\right)P(a=0)} = \frac{\left(\prod_{g_i \in G_P} P(g_i=1 \mid a=1)\right)\left(\prod_{g_i \in G_S} P(g_i=0 \mid a=1)\right)P(a=1)}{\left(\prod_{g_i \in G_P} P(g_i=1 \mid a=0)\right)\left(\prod_{g_i \in G_S} P(g_i=0 \mid a=0)\right)P(a=0)}$$

$$= \frac{P(g_i=1 \mid a=1)^{|G_P|}\, P(g_i=0 \mid a=1)^{|G_S|}\, P(a=1)}{P(g_i=1 \mid a=0)^{|G_P|}\, P(g_i=0 \mid a=0)^{|G_S|}\, P(a=0)}$$

We assume that all bound genes respond to TF activity in the same manner and estimate that 80% of genes that are bound by a TF that is active in the stress condition are affected by the binding (Supplementary Results). That is, $P(g_i = 1 \mid a = 1) = 0.8$ and $P(g_i = 0 \mid a = 1) = 0.2$. When the TF is not active, i.e. $(a = 0)$, the probability that a gene will be affected by the binding is given by the background distribution. The background distribution is given by the percentage of *all* genes (not just the set bound by *t*) along each path out of the split. $P(g_i = 1 \mid a = 0) = \frac{|O_P|}{|O_P \cup O_S|}$, where $O_P$ is the set of all genes that follow the primary path out of the split and $O_S$ is the set of all genes on a secondary path out of the split. Likewise,

$P(g_i = 0 \mid a = 0) = \frac{|O_S|}{|O_P \cup O_S|}$. Note that $O_P$ and $O_S$ exclude genes that are on another path and do not enter the split. Thus, the final activity score is

$$score(t,e) = \frac{0.8^{|G_P|}0.2^{|G_S|}P(a=1)}{\left(\frac{|O_P|}{|O_P \cup O_S|}\right)^{|G_P|}\left(\frac{|O_S|}{|O_P \cup O_S|}\right)^{|G_S|}P(a=0)}$$

The TF activity score at a particular iteration of SDREM is the maximum score achieved over all possible bifurcation events *e*. To determine the significance of a specific activity score we use a randomization method. We run DREM multiple times (10 for all analyses here) with protein-DNA binding data that has been randomized. This generates a distribution of random TF activity scores from which we select the top 50 activity scores from each randomized run. All TFs with *real* activity scores in the 50$^{th}$ or greater percentile in this distribution are considered active, and these TFs are used as targets during the subsequent network orientation. Because TF activity scores can take arbitrarily large values, we normalize them before incorporating them into the network orientation objective function. Activity scores are normalized by multiplying their percentile in the random distribution (not the score itself) by *k*, the maximum path length in the network orientation.

**Interaction network weighting**

All protein-protein interaction data was obtained from version 2.0.51 of BioGRID (Stark et al. 2006). The experimental method(s) used to detect interactions and number of times they were independently reported were used to weight all edges in the PPI network as previously described (Gitter et al. 2011), and only high-confidence edges with a weight of at least 0.6 were retained in

the network, as was done in this previous work. The interaction network also included protein-DNA edges, whose weights are provided in Supplementary Table S19.

**Supplementary Table S19. Protein-DNA interaction weights.** Condition refers to the condition in which the ChIP-chip experiment was performed, and conservation is the number of other yeast species in which the known binding motif is conserved.

| p-value threshold | Condition | Conservation | Weight |
|---|---|---|---|
| 0.001 | YPD | 2 | 0.95 |
| 0.001 | YPD | 1 | 0.8 |
| 0.001 | YPD | 0 | 0.6 |
| 0.005 | YPD | 2 | 0.7 |
| 0.005 | YPD | 1 | 0.5 |
| 0.005 | YPD | 0 | 0.3 |
| N/A | Osmotic stress | N/A | 0.9 |
| 0.001 | Rapamycin | N/A | 0.9 |
| 0.005 | Rapamycin | N/A | 0.6 |

Most existing approaches for weighting protein-DNA interactions are unable to simultaneously account for experimental p-value, binding motif conservation, and experimental condition, which all influence edge weights in our network. The Physical Network Models strategy, for instance, uses p-values alone. Like ResponseNet, we divide the protein-DNA interactions based on conservation of a binding motif if such a motif is present. ResponseNet arbitrarily assigns a weight of 0.7 to protein-DNA interactions with a binding motif conserved in at least 2 other yeast species (Yeger-Lotem et al. 2009). We instead elect to use 0.95 to be consistent with the weights of the highest confidence edges in our PPI network. The remaining categories of edges are assigned lower weights based on how ChIP-chip p-value, binding motif conservation, and condition-specificity translate to edge reliability (similar to our prior approach with the PPI network where an expert assigned various confidence scores to different experimental methods).

Protein-DNA interactions with p-values greater than 0.005 were discarded. The interaction networks used to build the osmotic stress and rapamycin models included the general interaction data plus either the osmotic stress or rapamycin binding data, respectively. The YPD data only includes interactions with known binding motifs (MacIsaac et al. 2006). The osmotic stress interactions were measured in cells treated with the salt KCl (Capaldi et al. 2008). There is no p-value threshold in Supplementary Table S19 for this dataset because only enrichment ratios are publicly available. To obtain a set of interactions, we used the thresholds provided in Fig. 4 of Capaldi *et al*, in which it was reported that 82 Sko1 targets and 35 Hot1 targets had a p-value less than 0.05 in their custom peak-fitting model. For each TF, we then selected this number of top-ranked genes from the ChIP-chip enrichment ratio dataset. For the rapamycin binding data (Harbison et al. 2004), p-values were available.

**Osmotic stress data and validation**

These 5 source proteins (Cdc42, Msb2, Sho1, Sln1, and Ste50) are the proteins in the *Science Signaling* Database of Cell Signaling HOG pathway representation that are upstream and do not have a parent node. In addition to the signaling databases (Supplementary Table S3), we compiled a set of osmotic stress responders by considering several resources. We included all genes that were annotated with decreased resistance to hyperosmotic stress in SGD (http://www.yeastgenome.org/cgi-bin/phenotype/phenotype.pl?rm=specific_tables&phenotype=hyperosmotic%20stress%20resistance:%20decreased). We also included genes if their deletion strains exhibited a fitness defect in sorbitol (Hillenmeyer et al. 2008). For this sorbitol screen, we required that at least one p-value across all replicates was less than $10^{-4}$. Finally, we searched the literature for proteins that were

previously identified to be associated with this response (see Supplementary Tables S1, S2, S4, and S5).

The osmotic stress analysis incorporated Hot1 and Sko1 ChIP-chip measurements in the presence of salt (Capaldi et al. 2008). Dynamic expression data collected from a wild type strain subjected to osmotic stress (0.4 M NaCl) was used to build the short model (Romero-Santacreu et al. 2009). All replicates were included in the analysis. The long model's expression data was from cells treated with sorbitol (Gasch et al. 2000). Although both datasets were collected after subjecting yeast cells to an osmotic stress, we analyze both due to the differences in the transcriptional responses observed. SDREM filters genes that are not differentially expressed, and of the 2707 genes that are differentially expressed in the short model and 2889 genes that are differentially expressed in the long model, only 1406 are present in both (making the similarity of the predicted network models quite remarkable).

The p-values reported for the overlaps between the short model predictions and the HOG gold standard were calculated using Fisher's exact test. We permissively define TFs to be any protein present in the ChIP-chip binding data (Harbison et al. 2004; Capaldi et al. 2008) with the exception of Hog1, a known MAPK. Under this definition, the gold standard contains 7 TFs, 28 of SDREM's predictions are TFs, and 4 of those predictions are in the gold standard. Our dataset included 203 TFs that could potentially be chosen by SDREM, and the p-values were calculated in this context. There were 30 non-TF SDREM predictions, 30 additional gold standard proteins, and 6 proteins in both sets. For this p-value calculation we considered 5245 possible proteins, which include all proteins in our physical interaction network and all gold

standard members. The 5 source proteins given as input to SDREM are excluded from this analysis. The p-value reported for the overlap between SDREM's predictions and the osmotic stress-related genes includes both the HOG gold standard members and genetic screen hits (from SGD and Hillenmeyer *et al* (Hillenmeyer et al. 2008)) in the positive set and considered all SDREM predictions (TFs and non-TFs) jointly. Additional predictions that were validated only in the literature search also were excluded from this calculation. The overlaps for the long model were calculated in the same manner.

**Microscopy**

Multiple repeats were collected for the control and sorbitol-exposed cells. However, only a single representative image with clearly defined cell boundaries was selected for significance testing. ImageJ (Abramoff et al. 2004) was used for all image post-processing and analysis. Background subtraction was performed using the default settings (the rolling ball algorithm with a 50 pixel radius) and the images were converted to grayscale. Regions of interest (ROIs) were manually defined to annotate the cell boundaries, and the standard deviation of pixel intensity from all ROIs in an image was extracted (Supplementary Fig. S5). Cells without distinct boundaries were excluded from the analysis. A one-tailed t-test assuming unequal variance and sample sizes was used to calculate p-values. Images in Fig. 4A are shown after background subtraction, and the original images are available on SDREM's supporting website.

**Flow cytometry**

All FACS replicates originally contained measurements from 50000 individual cells. Approximately half of these data points remained after filtering based on the FSC-A and SSC-A

values; similar filtering is customary in the analysis of FACS data (Bar-Even et al. 2006). Supplementary Table S20 shows how many outliers were removed in each replicate. In some of the Cin5 and Spt23 replicates, the protein expression before sorbitol treatment was lower than the background, which lead to negative fold change values. Experiments yielding negative fold change were excluded from subsequent analysis, which is why these two proteins were excluded from Fig. 4B. P-values for Gcn4, Hog1, and Rox1 were calculated using a paired one-tailed t-test, which tests the $\log_2$ mean background-subtracted protein expression levels (Supplementary Table S20). Biological replicates were paired according to the date of the experiments.

**Knockout analysis**

*ASF1*, *BEM1*, *FUS3*, *GAL11*, *PCL2*, and *RVS167* were selected for deletion due to their predicted role in the short model. However, most were important nodes in the oriented network of the long model as well. In addition, we excluded TFs from the set of potential knockout candidates and sought proteins that belonged to different levels of the signaling network hierarchy. That is, some proteins were further upstream whereas others were downstream and interact directly with transcription factors.

The Agilent scanner allows adjustment of the photomultiplier tube (PMT) sensitivity level. Our comparison of gene expression fold changes at PMT sensitivity levels of 10% and 100% showed that they were not substantially different, and we used the 10% scans for all subsequent analysis.

After scanning and processing per standard Agilent protocols (Agilent's Feature Extraction software version 10.7.3.1.), we removed probes for which the coefficient of variation was greater

than 40%. For all microarray data we applied probe location normalization that is based on a Gaussian image filtering technique to correct for spatial bias, which was followed by quantile normalization. For each array we removed control probes and aggregated the data to the gene level by taking the median expression level of all probes that corresponded to a particular gene.

Genes that were not differentially expressed in the wild type osmotic stress datasets were excluded from further analysis. Because different genes were differentially expressed in the two wild type datasets, we generated two knockout datasets for further processing. For the short model, we required the wild type $\log_2$ differential expression to have magnitude of at least 1 and did not allow missing data. This resulted in a set of 2655 genes (Supplementary Table S21) – slightly fewer than the number of genes used to build the regulatory paths in SDREM where missing data was allowed – of which 2624 were also on the arrays used for our knockouts. For the long model, the $\log_2$ expression threshold was set to 0.5 and missing data was not allowed, yielding a set of 2858 genes. Of these, 2784 were on our arrays (Supplementary Table S21).

We then used significance analysis of microarrays (SAM) (Tusher et al. 2001) to identify significantly differentially expressed genes in the knockout data. SAM was run using the two class unpaired response type, 1000 permutations, and default values for all other settings. We set the delta parameter to the value that gave a false discovery rate of at most 0.2. In addition, we required that significant genes had a minimum twofold change in expression. SAM produced sets of significant up- and down-regulated genes that met these criteria. The distinct sets of up- and down-regulated genes obtained from SAM were analyzed separately. Because SAM imputes missing data, we eliminated genes for which all of the control readings or both of the

knockout replicate expression levels were missing from the sets of significant genes. The SAM software depends on the statconnDCOM tool (Baier and Neuwirth 2007).

Although SAM does not take log ratios as input, we also calculated $\log_2$ differential expression for the knockouts in order to facilitate reuse of the data. After normalizing the data, we took the median of the two replicates per knockout and the replicates per control strain. Log ratios were not calculated for genes in which expression levels across the replicates differed substantially (i.e. the $\log_2$ absolute expression levels disagreed by more than 1.5). When four control replicates per gene where available, if only one replicate disagreed with the others then it was discarded and the log ratio was calculated using the other three. The raw and normalized microarray data are available from GEO under accession number GSE28213.

To identify which knockouts affected genes that overlapped significantly with the genes on SDREM regulatory paths, we used Fisher's exact test. The results from the knockout dataset that was filtered using the short osmotic stress wild type expression data were only compared to the short model, and the same is true for the long osmotic stress expression data and model. Rather than use the all yeast genes as the set of all genes in Fisher's exact test, we only use those genes that are affected by sorbitol, which yields conservative (larger) p-values. The overlaps were calculated separately for the up- and down-regulated genes, and p-values were multiplied by the number of regulatory paths (10 for the short model and 9 for the long model) to correct for multiple hypothesis testing. Fig. 5B and Supplementary Fig. S6B – S8 associate a protein with a regulatory path if either its differentially activated or repressed genes overlap the path with a corrected p-value less than 0.05. For the osmotic stress-specific overlap analysis, all 868 general

environmental stress response genes (Gasch et al. 2000) were removed from the sets of genes on the regulatory paths and the knockout-affected genes before calculating the overlaps and their significance in the same manner (Supplementary Table S21).

To calculate the significance of the number of regulatory paths that significantly overlap with one or more knockouts, we recalculated the overlaps using random regulatory paths. These random regulatory paths contained the same number of genes on each path as the real regulatory paths, but the gene assignment to paths was random. The same set of genes was used for the real and random paths. We than calculated the number of random paths that significantly overlap one or more knockouts with a corrected p-value $\leq 0.05$, and used these counts to determine the p-values of the real enrichment. For the osmotic stress-specific analysis, the procedure was identical except all ESR genes were filtered from the regulatory paths and knockout effects.

**TOR data and validation**

Urban *et al* (Urban et al. 2007) studied the effects of rapamycin in several yeast strains, and we used the dynamic expression data from the wild type strain with a $\log_2$ fold change threshold of 1. The extended gold standard data sources were described in the Supplementary Results. For the Hillenmeyer *et al* rapamycin screen (Hillenmeyer et al. 2008), we required that in at least one of the seven replicates the p-value was less than $10^{-4}$ (Supplementary Results). The p-value of the overlap between SDREM predictions and the rapamycin extended gold standard was calculated using Fisher's exact test. Twenty-one of the 48 predictions were in the extended gold standard, which contained 1576 unique genes. We considered 6446 possible genes, which includes all genes in our physical interaction network and all extended gold standard members.

Ten additional predictions that were validated only in the literature search were excluded from this calculation.

### *Arabidopsis thaliana* data, settings, and evaluation

Unlike the yeast analysis, the *Arabidopsis* interaction network included host-pathogen PPI (Mukhtar et al. 2011) and *Arabidopsis* PPI (Arabidopsis Interactome Mapping Consortium 2011) but not the protein-DNA interactions (Yilmaz et al. 2011) that were used to learn the regulatory paths. The interaction network also used a uniform weight of 0.75 because the types of evidence used to weight the yeast interaction network were not available. All *Hpa* effectors were used as sources, and families of effectors were grouped as in the original data (Mukhtar et al. 2011). A $\log_2$ fold change threshold of 0.5 was used for the temporal expression data (Wang et al. 2011) and no missing values were allowed. The p-value for the overlap with the functionally validated *Arabidopsis* immune responders was calculated with respect to all proteins in the PPI network (i.e. all possible proteins SDREM could predict). The Gene Ontology (Ashburner et al. 2000) analysis was performed using DAVID (Huang et al. 2009a, 2009b).

### Physical Network Models, ResponseNet, and GeneReg settings

Although Physical Network Models and ResponseNet are both capable of linking sources and targets in a physical interaction network, they were not designed to connect upstream proteins in a signaling network to dynamic transcriptional effects. Therefore, comparing them with SDREM requires running them in an untraditional manner or preprocessing the input data to emulate the types of input they expect (Methods). We ran PNM using the default physical interaction network provided with its code because all trials that used our interaction network produced an

empty set of predictions. This may be due to the much higher weights used in the PNM-provided network. Although SDREM finds source-target paths with up to 5 edges, we set the maximum path length for PNM to 4 because it was previously shown that PNM does not terminate in a reasonable time when run on the yeast interactome with a path length of 5 (Gitter et al. 2011).

We ran ReponseNet via the ResponseNet web server (Lan et al. 2011), which takes as input a set of sources and set of targets. For the sources, we used the 5 HOG pathway sources and did not assign weights so that the default uniform weights would be applied. The user may optionally provide the PPI and protein-DNA interaction networks, and we uploaded the same weighted networks used in the SDREM analysis.

We ran GeneReg on the long osmotic stress dataset, using the expression profiles of all genes that are not missing data and exceed a $\log_2$ fold change threshold of 0.5 in one or more time points (the same threshold was used for SDREM). In the example GeneReg analysis (Huang et al. 2010), B-spline interpolation was applied to transform 30 time points into 100. We similarly used B-spline interpolation to expand the osmotic stress dataset from 6 to 20 time points (approximately a threefold change). The list of 47 potential regulators provided to GeneReg was created by intersecting the TFs in our protein-DNA dataset (MacIsaac et al. 2006; Capaldi et al. 2008) with the TFs that were differentially expressed. Default values were used for the adjusted $R^2$ cutoff, the maximum and minimum regulator coefficients, and all other parameters. The p-values for the HOG TF overlap were calculated with respect to all yeast TFs (Harbison et

al. 2004) (the same TFs used to calculate the p-values for SDREM), not the subset of TFs that were differentially expressed.

**Supplementary Table S20**

This table is a separate Excel spreadsheet that contains the mean protein expression levels from all FACS experiments that were used to calculate fold change for Fig. 4B.

**Supplementary Table S21**

This table is a separate Excel spreadsheet that contains the significance of the overlaps between knockout-affected genes and the SDREM regulatory paths. The table also shows the overlaps between the TFs downstream of the knockouts in the oriented interaction network and the active TFs on the regulatory paths. Lastly, it lists osmotic stress-specific genes used to calculate the overlaps between the knockout-affected genes and regulatory paths.

## Supplementary References


Abramoff MD, Magelhaes PJ, and Ram SJ. 2004. Image processing with ImageJ. *Biophotonics Int* **11**: 36–42.

Arabidopsis Interactome Mapping Consortium. 2011. Evidence for network evolution in an Arabidopsis interactome map. *Science* **333**: 601–607.

Ashburner M, Ball CA, Blake JA, Botstein D, Butler H, Cherry JM, Davis AP, Dolinski K, Dwight SS, Eppig JT, et al. 2000. Gene Ontology: tool for the unification of biology. *Nat Genet* **25**: 25–29.

Baier T, and Neuwirth E. 2007. Excel :: COM :: R. *Comput Stat* **22**: 91–108.

Balasubramaniyan R, Hullermeier E, Weskamp N, and Kamper J. 2005. Clustering of gene expression data using a local shape-based similarity measure. *Bioinformatics* **21**: 1069–1077.

Bar-Even A, Paulsson J, Maheshri N, Carmi M, O'Shea E, Pilpel Y, and Barkai N. 2006. Noise in protein expression scales with natural protein abundance. *Nat Genet* **38**: 636–643.

Bar-Joseph Z, Gerber GK, Lee TI, Rinaldi NJ, Yoo JY, Robert F, Gordon DB, Fraenkel E, Jaakkola TS, Young RA, et al. 2003. Computational discovery of gene modules and regulatory networks. *Nat Biotechnol* **21**: 1337–1342.

Bauer F, Urdaci M, Aigle M, and Crouzet M. 1993. Alteration of a yeast SH3 protein leads to conditional viability with defects in cytoskeletal and budding patterns. *Mol Cell Biol* **13**: 5070–5084.

Bellí G, Garí E, Aldea M, and Herrero E. 2001. Osmotic stress causes a G1 cell cycle delay and downregulation of Cln3/Cdc28 activity in Saccharomyces cerevisiae. *Mol Microbiol* **39**: 1022–1035.

Capaldi AP, Kaplan T, Liu Y, Habib N, Regev A, Friedman N, and O'Shea EK. 2008. Structure and function of a transcriptional network activated by the MAPK Hog1. *Nat Genet* **40**: 1300–1306.

Chan T-F, Carvalho J, Riles L, and Zheng XFS. 2000. A chemical genomics approach toward understanding the global functions of the target of rapamycin protein (TOR). *Proc Natl Acad Sci USA* **97**: 13227 –13232.

Cutler NS, Pan X, Heitman J, and Cardenas ME. 2001. The TOR Signal Transduction Cascade Controls Cellular Differentiation in Response to Nutrients. *Mol Biol Cell* **12**: 4103–4113.

Flatauer LJ, Zadeh SF, and Bardwell L. 2005. Mitogen-Activated Protein Kinases with Distinct Requirements for Ste5 Scaffolding Influence Signaling Specificity in Saccharomyces cerevisiae. *Mol Cell Biol* **25**: 1793–1803.

Gasch AP, Spellman PT, Kao CM, Carmel-Harel O, Eisen MB, Storz G, Botstein D, and Brown PO. 2000. Genomic Expression Programs in the Response of Yeast Cells to Environmental Changes. *Mol Biol Cell* **11**: 4241–4257.

Gitter A, Klein-Seetharaman J, Gupta A, and Bar-Joseph Z. 2011. Discovering pathways by orienting edges in protein interaction networks. *Nucleic Acids Res* **39**: e22.

Goossens A, Dever TE, Pascual-Ahuir A, and Serrano R. 2001. The Protein Kinase Gcn2p Mediates Sodium Toxicity in Yeast. *J Biol Chem* **276**: 30753 –30760.

Haitani Y, Shimoi H, and Takagi H. 2006. Rsp5 regulates expression of stress proteins via post-translational modification of Hsf1 and Msn4 in Saccharomyces cerevisiae. *FEBS Lett* **580**: 3433–3438.

Hao N, Zeng Y, Elston TC, and Dohlman HG. 2008. Control of MAPK Specificity by Feedback Phosphorylation of Shared Adaptor Protein Ste50. *J Biol Chem* **283**: 33798 –33802.

Harbison CT, Gordon DB, Lee TI, Rinaldi NJ, Macisaac KD, Danford TW, Hannett NM, Tagne J-B, Reynolds DB, Yoo J, et al. 2004. Transcriptional regulatory code of a eukaryotic genome. *Nature* **431**: 99–104.

Hillenmeyer ME, Fung E, Wildenhain J, Pierce SE, Hoon S, Lee W, Proctor M, St. Onge RP, Tyers M, Koller D, et al. 2008. The chemical genomic portrait of yeast: uncovering a phenotype for all genes. *Science* **320**: 362–365.

Hohmann S. 2009. Control of high osmolarity signalling in the yeast Saccharomyces cerevisiae. *FEBS Lett* **583**: 4025–4029.

Hohmann S, Krantz M, and Nordlander B. 2007. Yeast Osmoregulation. *Methods Enzymol* **428**: 29–45.

Huang DW, Sherman BT, and Lempicki RA. 2009a. Bioinformatics enrichment tools: paths toward the comprehensive functional analysis of large gene lists. *Nucleic Acids Res* **37**: 1–13.

Huang DW, Sherman BT, and Lempicki RA. 2009b. Systematic and integrative analysis of large gene lists using DAVID bioinformatics resources. *Nat Protoc* **4**: 44–57.

Huang T, Liu L, Qian Z, Tu K, Li Y, and Xie L. 2010. Using GeneReg to construct time delay gene regulatory networks. *BMC Res Notes* **3**: 142.

Kanehisa M, and Goto S. 2000. KEGG: kyoto encyclopedia of genes and genomes. *Nucleic Acids Res* **28**: 27–30.

Kim S, and Shah K. 2007. Dissecting yeast Hog1 MAP kinase pathway using a chemical genetic approach. *FEBS Lett* **581**: 1209–1216.

Kim Y-A, Wuchty S, and Przytycka TM. 2011. Identifying Causal Genes and Dysregulated Pathways in Complex Diseases. *PLoS Comput Biol* **7**: e1001095.

Klopf E, Paskova L, Solé C, Mas Gloria, Petryshyn A, Posas F, Wintersberger U, Ammerer G, and Schüller C. 2009. Cooperation between the INO80 Complex and Histone Chaperones Determines Adaptation of Stress Gene Transcription in the Yeast Saccharomyces cerevisiae. *Mol Cell Biol* **29**: 4994–5007.

Krantz M, Ahmadpour D, Ottosson L-G, Warringer J, Waltermann C, Nordlander B, Klipp E, Blomberg A, Hohmann S, and Kitano H. 2009. Robustness and fragility in the yeast high osmolarity glycerol (HOG) signal-transduction pathway. *Mol Syst Biol* **5**.

Kuranda K, Leberre V, Sokol S, Palamarczyk G, and Francois J. 2006. Investigating the caffeine effects in the yeast Saccharomyces cerevisiae brings new insights into the connection between TOR, PKC and Ras/cAMP signalling pathways. *Mol Microbiol* **61**: 1147–1166.

Kusari AB, Molina DM, Sabbagh W, Lau CS, and Bardwell L. 2004. A conserved protein interaction network involving the yeast MAP kinases Fus3 and Kss1. *J Cell Biol* **164**: 267–277.

Lan A, Smoly IY, Rapaport G, Lindquist S., Fraenkel E., and Yeger-Lotem E. 2011. ResponseNet: revealing signaling and regulatory networks linking genetic and transcriptomic screening data. *Nucleic Acids Res* **39**: W424–W429.

Lee J, Colwill K, Aneliunas V, Tennyson C, Moore L, Ho Y, and Andrews B. 1998. Interaction of yeast Rvs167 and Pho85 cyclin-dependent kinase complexes may link the cell cycle to the actin cytoskeleton. *Curr Biol* **8**: 1310–1321, S1.

Lin L-H, Lee H-C, Li W-H, and Chen B-S. 2007. A systematic approach to detecting transcription factors in response to environmental stresses. *BMC Bioinformatics* **8**: 473.

MacIsaac K, Wang T, Gordon DB, Gifford D, Stormo GD, and Fraenkel Ernest. 2006. An improved map of conserved regulatory sites for Saccharomyces cerevisiae. *BMC Bioinformatics* **7**: 113.

Madden K, Sheu Y-J, Baetz K, Andrews B, and Snyder M. 1997. SBF Cell Cycle Regulator as a Target of the Yeast PKC-MAP Kinase Pathway. *Science* **275**: 1781 –1784.

Martin DE, Soulard A, and Hall MN. 2004. TOR Regulates Ribosomal Protein Gene Expression via PKA and the Forkhead Transcription Factor FHL1. *Cell* **119**: 969–979.

Mas Glòria, de Nadal E, Dechant R, de la Concepción MLR, Logie C, Jimeno-González S, Chávez S, Ammerer G, and Posas F. 2009. Recruitment of a chromatin remodelling complex by the Hog1 MAP kinase to stress genes. *EMBO J* **28**: 326–336.

Mazor Y, and Kupiec M. 2009. Developmentally regulated MAPK pathways modulate heterochromatin in Saccharomyces cerevisiae. *Nucleic Acids Res* **37**: 4839 –4849.

McClean MN, Mody A, Broach JR, and Ramanathan S. 2007. Cross-talk and decision making in MAP kinase pathways. *Nat Genet* **39**: 409–414.

Miller C, Schwalb B, Maier K, Schulz D, Dümcke S, Zacher B, Mayer A, Sydow J, Marcinowski L, Dölken L, et al. 2011. Dynamic transcriptome analysis measures rates of mRNA synthesis and decay in yeast. *Mol Syst Biol* **7**.

Mukhtar MS, Carvunis A-R, Dreze M, Epple P, Steinbrenner J, Moore J, Tasan M, Galli M, Hao T, Nishimura MT, et al. 2011. Independently Evolved Virulence Effectors Converge Onto Hubs in a Plant Immune System Network. *Science* **333**: 596–601.

de Nadal E, and Posas F. 2010. Multilayered control of gene expression by stress-activated protein kinases. *EMBO J* **29**: 4–13.

Nakashima A, Maruki Y, Imamura Y, Kondo C, Kawamata T, Kawanishi I, Takata H, Matsuura A, Lee KS, Kikkawa U, et al. 2008. The Yeast Tor Signaling Pathway Is Involved in G2/M Transition via Polo-Kinase. *PLoS One* **3**: e2223.

Natarajan K, Meyer MR, Jackson BM, Slade D, Roberts C, Hinnebusch AG, and Marton MJ. 2001. Transcriptional Profiling Shows that Gcn4p Is a Master Regulator of Gene Expression during Amino Acid Starvation in Yeast. *Mol Cell Biol* **21**: 4347–4368.

Nevitt T, Pereira J, Azevedo D, Guerreiro P, and Rodrigues-Pousada C. 2004. Expression of YAP4 in Saccharomyces cerevisiae under osmotic stress. *Biochem J* **379**: 367–374.

Ni L, Bruce C, Hart C, Leigh-Bell J, Gelperin D, Umansky L, Gerstein MB, and Snyder M. 2009. Dynamic and complex transcription factor binding during an inducible response in yeast. *Genes Dev* **23**: 1351 –1363.

O'Rourke SM, Herskowitz I, and O'Shea EK. 2002. Yeast go the whole HOG for the hyperosmotic response. *Trends Genet* **18**: 405–412.

Pokholok DK, Zeitlinger J, Hannett NM, Reynolds DB, and Young RA. 2006. Activated Signal Transduction Kinases Frequently Occupy Target Genes. *Science* **313**: 533 –536.

Proft M, Gibbons FD, Copeland M, Roth FP, and Struhl K. 2005. Genomewide Identification of Sko1 Target Promoters Reveals a Regulatory Network That Operates in Response to Osmotic Stress in Saccharomyces cerevisiae. *Eukaryot Cell* **4**: 1343–1352.

Rodríguez-Peña JM, García R, Nombela C, and Arroyo J. 2010. The high-osmolarity glycerol (HOG) and cell wall integrity (CWI) signalling pathways interplay: a yeast dialogue between MAPK routes. *Yeast* **27**: 495–502.

Romero-Santacreu L, Moreno J, Pérez-Ortín JE, and Alepuz P. 2009. Specific and global regulation of mRNA stability during osmotic stress in Saccharomyces cerevisiae. *RNA* **15**: 1110 –1120.

Schmelzle T, Beck T, Martin DE, and Hall MN. 2004. Activation of the RAS/Cyclic AMP Pathway Suppresses a TOR Deficiency in Yeast. *Mol Cell Biol* **24**: 338–351.

Schmitt WA, Raab RM, and Stephanopoulos G. 2004. Elucidation of Gene Interaction Networks Through Time-Lagged Correlation Analysis of Transcriptional Data. *Genome Res* **14**: 1654–1663.

Scott S, Abul-Hamd AT, and Cooper TG. 2000. Roles of the Dal82p Domains in Allophanate/Oxalurate-dependent Gene Expression in Saccharomyces cerevisiae. *J Biol Chem* **275**: 30886 –30893.

Shock TR, Thompson J, Yates JR, and Madhani HD. 2009. Hog1 Mitogen-Activated Protein Kinase (MAPK) Interrupts Signal Transduction between the Kss1 MAPK and the Tec1 Transcription Factor To Maintain Pathway Specificity. *Eukaryot Cell* **8**: 606–616.

Stark C, Breitkreutz B-J, Reguly T, Boucher L, Breitkreutz A, and Tyers M. 2006. BioGRID: a general repository for interaction datasets. *Nucleic Acids Res* **34**: D535–539.

Truman AW, Kim K-Y, and Levin DE. 2009. Mechanism of Mpk1 Mitogen-Activated Protein Kinase Binding to the Swi4 Transcription Factor and Its Regulation by a Novel Caffeine-Induced Phosphorylation. *Mol Cell Biol* **29**: 6449–6461.

Tsang CK, Bertram PG, Ai W, Drenan R, and Zheng XFS. 2003. Chromatin-mediated regulation of nucleolar structure and RNA Pol I localization by TOR. *EMBO J* **22**: 6045–6056.

Tusher VG, Tibshirani R, and Chu G. 2001. Significance analysis of microarrays applied to the ionizing radiation response. *Proc Natl Acad Sci USA* **98**: 5116 –5121.

Urban J, Soulard A, Huber A, Lippman S, Mukhopadhyay D, Deloche O, Wanke V, Anrather D, Ammerer G, Riezman H, et al. 2007. Sch9 Is a Major Target of TORC1 in Saccharomyces cerevisiae. *Mol Cell* **26**: 663–674.

Vyas VK, Berkey CD, Miyao T, and Carlson M. 2005. Repressors Nrg1 and Nrg2 Regulate a Set of Stress-Responsive Genes in Saccharomyces cerevisiae. *Eukaryot Cell* **4**: 1882–1891.

Wade JT, Hall DB, and Struhl K. 2004. The transcription factor Ifh1 is a key regulator of yeast ribosomal protein genes. *Nature* **432**: 1054–1058.

Wang W, Barnaby JY, Tada Y, Li H, Tör M, Caldelari D, Lee D, Fu X-D, and Dong X. 2011. Timing of plant immune responses by a central circadian regulator. *Nature* **470**: 110–114.

Winters MJ, and Pryciak PM. 2005. Interaction with the SH3 Domain Protein Bem1 Regulates Signaling by the Saccharomyces cerevisiae p21-Activated Kinase Ste20. *Mol Cell Biol* **25**: 2177–2190.

Wu W-S, Li W-H, and Chen B-S. 2008. Reconstructing a Network of Stress-Response Regulators via Dynamic System Modeling of Gene Regulation. *Gene Regul Syst Bio* **2**: 53–62.

Xiao L, and Grove A. 2009. Coordination of Ribosomal Protein and Ribosomal RNA Gene Expression in Response to TOR Signaling. *Curr Genomics* **10**: 198–205.

Xie MW, Jin F, Hwang H, Hwang S, Anand V, Duncan MC, and Huang J. 2005. Insights into TOR function and rapamycin response: Chemical genomic profiling by using a high-density cell array method. *Proc Natl Acad Sci USA* **102**: 7215 –7220.

Yeger-Lotem E, Riva L, Su LJ, Gitler AD, Cashikar AG, King OD, Auluck PK, Geddie ML, Valastyan JS, Karger DR, et al. 2009. Bridging high-throughput genetic and transcriptional data reveals cellular responses to alpha-synuclein toxicity. *Nat Genet* **41**: 316–323.

Yilmaz A, Mejia-Guerra MK, Kurz K, Liang X, Welch L, and Grotewold E. 2011. AGRIS: the Arabidopsis Gene Regulatory Information Server, an update. *Nucleic Acids Res* **39**: D1118–D1122.

Yu VPCC, and Reed SI. 2004. Cks1 is Dispensable for Survival in Saccharomyces cerevisiae. *Cell Cycle* **3**: 1402–1404.

Zaman S, Lippman SI, Zhao X, and Broach JR. 2008. How Saccharomyces Responds to Nutrients. *Annu Rev Genet* **42**: 27–81.

Zapater M, Sohrmann M, Peter M, Posas F, and de Nadal E. 2007. Selective Requirement for SAGA in Hog1-Mediated Gene Expression Depending on the Severity of the External Osmostress Conditions. *Mol Cell Biol* **27**: 3900–3910.

Zhu M, and Wang Y. 2009. Rapamycin enhances G protein signaling in the budding yeast Saccharomyces Cerevisiae. *FASEB J* **23**: 530.9.

Zinzalla V, Graziola M, Mastriani A, Vanoni M, and Alberghina L. 2007. Rapamycin-mediated G1 arrest involves regulation of the Cdk inhibitor Sic1 in Saccharomyces cerevisiae. *Mol Microbiol* **63**: 1482–1494.

Zoppoli P, Morganella S, and Ceccarelli M. 2010. TimeDelay-ARACNE: Reverse engineering of gene networks from time-course data by an information theoretic approach. *BMC Bioinformatics* **11**: 154.